
Sampling with Mirrored Stein Operators

Jiabin Shi Microsoft Research Cambridge, MA jiabinshi@microsoft.com	Chang Liu Microsoft Research Beijing chang.liu@microsoft.com	Lester Mackey Microsoft Research Cambridge, MA lmackey@microsoft.com
---	--	--

Abstract

We introduce a new family of particle evolution samplers suitable for constrained domains and non-Euclidean geometries. Stein Variational Mirror Descent and Mirrored Stein Variational Gradient Descent minimize the Kullback-Leibler (KL) divergence to constrained target distributions by evolving particles in a dual space defined by a mirror map. Stein Variational Natural Gradient exploits non-Euclidean geometry to more efficiently minimize the KL divergence to unconstrained targets. We derive these samplers from a new class of mirrored Stein operators and adaptive kernels developed in this work. We demonstrate that these new samplers yield accurate approximations to distributions on the simplex, deliver valid confidence intervals in post-selection inference, and converge more rapidly than prior methods in large-scale unconstrained posterior inference. Finally, we establish the convergence of our new procedures under verifiable conditions on the target distribution.

1 Introduction

Accurately approximating an unnormalized distribution with a discrete sample is a fundamental challenge in machine learning, probabilistic inference, and Bayesian inference. Particle evolution methods like Stein variational gradient descent [SVGD, 44] tackle this challenge by applying deterministic updates to particles using operators based on Stein’s method [60, 26, 51, 45, 13, 27] and reproducing kernels [6] to sequentially minimize Kullback-Leibler (KL) divergence. SVGD has found great success in approximating unconstrained distributions for probabilistic learning [21, 30, 39] but breaks down for constrained targets, like distributions on the simplex [53] or the targets of post-selection inference [62, 40, 63], and fails to exploit informative non-Euclidean geometry [2].

In this work, we derive a family of particle evolution samplers suitable for target distributions with constrained domains and non-Euclidean geometries. Our development draws inspiration from mirror descent (MD) [50], a first-order optimization method that generalizes gradient descent with non-Euclidean geometry. To sample from a distribution with constrained support, our method first maps particles to a dual space. There, we update particle locations using a new class of *mirrored Stein operators* and adaptive reproducing kernels introduced in this work. Finally, the dual particles are mapped back to sample points in the original space, ensuring that all constraints are satisfied. We illustrate this procedure in Fig. 1. In Sec. 3, we develop two algorithms – Mirrored SVGD (MSVGD) and Stein Variational Mirror Descent (SVMD) – with different updates in the dual space; when only a single particle is used, MSVGD reduces to gradient ascent on the log dual space density, and SVMD reduces to mirror ascent on the log target density. In addition, by exploiting the connection between MD and natural gradient descent [2, 54], we develop a third algorithm – Stein Variational Natural Gradient (SVNG) – that extends SVMD to unconstrained targets with non-Euclidean geometry.

In Sec. 5, we demonstrate the advantages of our algorithms on benchmark simplex-constrained problems from the literature, constrained sampling problems in post-selection inference [62, 40, 63], and unconstrained large-scale posterior inference with the Fisher information metric. Finally, we analyze the convergence of our mirrored algorithms in Sec. 6 and discuss our results in Sec. 7.

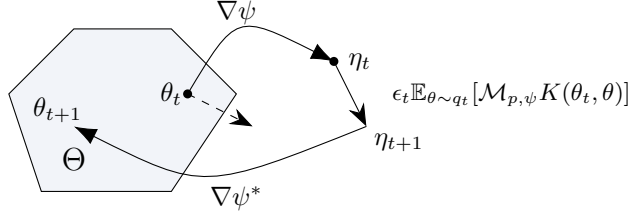


Figure 1: Updating particle approximations in constrained domains Θ . Standard updates like SVGD (dashed arrow) can push particles outside of the support. Our mirrored Stein updates in Alg. 1 (solid arrows) preserve the support by updating particles in a dual space and mapping back to Θ .

Related work Our mirrored Stein operators (7) are instances of diffusion Stein operators in the sense of [27], but their specific properties have not been studied, nor have they been used to develop sampling algorithms. There is now a large body of work on transferring algorithmic ideas from optimization to sampling [see, e.g., 14, 67, 18, 47, 59]. The closest to our work in this space is the recent marriage of mirror descent and MCMC. For example, Hsieh et al. [34] propose to run Langevin Monte Carlo (LMC, an Euler discretization of the Langevin diffusion) in a mirror space. Zhang et al. [70] analyze the convergence properties of the mirror-Langevin diffusion, Chewi et al. [12] demonstrate its advantages over the Langevin diffusion when using a Newton-type metric, and Ahn and Chewi [1] study its discretization for MCMC sampling in constrained domains. Relatedly, Patterson and Teh [53] proposed stochastic Riemannian LMC for sampling on the simplex.

Several modifications of SVGD have been proposed to incorporate geometric information. Riemannian SVGD [RSVG, 42] generalizes SVGD to Riemannian manifolds, but, even with the same metric tensor, their updates are more complex than ours, do not operate in a mirror space, require higher-order kernel derivatives, and reportedly do not perform well when with scalable stochastic estimates of $\nabla \log p$. Stein Variational Newton [SVN, 15, 9] introduces second-order information into SVGD. Their algorithm requires an often expensive Hessian computation and need not lead to descent directions, so inexact approximations are employed in practice. Our SVNG can be seen as an instance of matrix SVGD [MatSVG, 66] with an adaptive time-dependent kernel discussed in Sec. 4.4, a choice that is not explored in [66] and which recovers natural gradient descent when $n = 1$ unlike the heuristic kernel constructions of [66]. None of the aforementioned works provide convergence guarantees, and neither SVN nor matrix SVGD deals with constrained domains.

2 Background

2.1 Mirror descent and non-Euclidean geometry

Standard gradient descent can be viewed as optimizing a local quadratic approximation to the target function f : $\theta_{t+1} = \operatorname{argmin}_{\theta \in \Theta} \nabla f(\theta_t)^\top \theta + \frac{1}{2\epsilon_t} \|\theta - \theta_t\|_2^2$. When $\Theta \subseteq \mathbb{R}^d$ is constrained, it can be advantageous to replace $\|\cdot\|_2$ with a function Ψ that reflects the geometry of a problem [50, 5]:

$$\theta_{t+1} = \operatorname{argmin}_{\theta \in \Theta} \nabla f(\theta_t)^\top \theta + \frac{1}{\epsilon_t} \Psi(\theta, \theta_t). \quad (1)$$

We consider the mirror descent algorithm [50, 5] which chooses Ψ to be the Bregman divergence induced by a strictly convex function $\psi : \Theta \rightarrow \mathbb{R} \cup \{\infty\}$: $\Psi(\theta, \theta') = \psi(\theta) - \psi(\theta') - \nabla \psi(\theta')^\top (\theta - \theta')$. When Θ is a $(d+1)$ -simplex $\{\theta : \sum_{i=1}^d \theta_i \leq 1 \text{ and } \theta_i \geq 0 \text{ for } i \in [d]\}$, a common choice of ψ is the negative entropy $\psi(\theta) = \sum_{i=1}^{d+1} \theta_i \log \theta_i$, for $\theta_{d+1} \triangleq 1 - \sum_{i=1}^d \theta_i$. The solution of (1) is given by

$$\theta_{t+1} = \nabla \psi^*(\nabla \psi(\theta_t) - \epsilon_t \nabla f(\theta_t)), \quad (2)$$

where $\psi^*(\eta) \triangleq \sup_{\theta \in \Theta} \eta^\top \theta - \psi(\theta)$ is the convex conjugate of ψ and $\nabla \psi$ is a bijection from Θ to $\operatorname{dom}(\psi^*)$ with inverse map $(\nabla \psi)^{-1} = \nabla \psi^*$. We can view the update in (2) as first mapping θ_t to η_t by $\nabla \psi$, applying the update $\eta_{t+1} = \eta_t - \epsilon_t \nabla f(\theta_t)$, and mapping back through $\theta_{t+1} = \nabla \psi^*(\eta_{t+1})$.

Mirror descent can also be viewed as a discretization of the continuous-time dynamics $d\eta_t = -\nabla f(\theta_t) dt$, $\theta_t = \nabla \psi^*(\eta_t)$, which is equivalent to the Riemannian gradient flow

$$d\theta_t = -\nabla^2 \psi(\theta_t)^{-1} \nabla f(\theta_t) dt, \quad \text{or equivalently,} \quad d\eta_t = -\nabla^2 \psi^*(\eta_t)^{-1} \nabla_{\eta_t} f(\nabla \psi^*(\eta_t)) dt, \quad (3)$$

where $\nabla^2\psi(\theta)$ and $\nabla^2\psi^*(\eta)$ are Riemannian metric tensors (see App. A). In information geometry, the discretization of (3) is known as *natural gradient* descent [2]. There is considerable theoretical and practical evidence [48] showing that natural gradient works efficiently in learning.

2.2 Mirror-Langevin diffusions

Next we review the (overdamped) Langevin diffusion – a Markov process that underlies SVGD and many recent advances in Stein’s method – along with its recent mirrored generalization. The Langevin diffusion with equilibrium density p on \mathbb{R}^d is a Markov process $(\theta_t)_{t \geq 0} \subset \mathbb{R}^d$ satisfying the stochastic differential equation (SDE) $d\theta_t = \nabla \log p(\theta_t)dt + \sqrt{2}dB_t$ with $(B_t)_{t \geq 0}$ a standard Brownian motion [7, Sec. 4.5]. The Riemannian Langevin diffusion [53, 69, 46] extends the Langevin to non-Euclidean geometries encoded in a positive definite *metric tensor* $G(\theta)$:

$$d\theta_t = (G(\theta_t)^{-1}\nabla \log p(\theta_t) + \nabla \cdot G(\theta_t)^{-1})dt + \sqrt{2}G(\theta_t)^{-1/2}dB_t.^1$$

We show in App. B that the choice $G = \nabla^2\psi$ yields the recent mirror-Langevin diffusion [70, 12]

$$\theta_t = \nabla\psi^*(\eta_t), \quad d\eta_t = \nabla \log p(\theta_t)dt + \sqrt{2}\nabla^2\psi(\theta_t)^{1/2}dB_t. \quad (4)$$

3 Stein’s Identity and Mirrored Stein Operators

Stein’s identity [60] is a tool for characterizing a target distribution P using a so-called *Stein operator*. Hereafter, we assume P has a differentiable density p with convex support $\Theta \subseteq \mathbb{R}^d$. A Stein operator \mathcal{S}_p takes as input functions g from a *Stein set* \mathcal{G} and outputs mean-zero functions under p :

$$\mathbb{E}_p[(\mathcal{S}_p g)(\theta)] = 0, \quad \text{for all } g \in \mathcal{G}. \quad (5)$$

To identify Stein operators for broad classes of targets p , Gorham and Mackey [26] proposed to build upon Barbour’s generator method [3]. First, identify a Markov process $(\theta_t)_{t \geq 0}$ that has p as the equilibrium density; Gorham and Mackey [26] chose the Langevin diffusion of Sec. 2.2. Next, build a Stein operator based on the (infinitesimal) generator A of the process [52, Def. 7.3.1]:

$$(Af)(\theta) = \lim_{t \rightarrow 0} \frac{1}{t}(\mathbb{E}f(\theta_t) - \mathbb{E}f(\theta_0)) \quad \text{for } f : \mathbb{R}^d \rightarrow \mathbb{R},$$

as the generator outputs mean-zero functions under p under relatively mild conditions; the resulting *Langevin Stein operator* of [26] is given by

$$(\mathcal{S}_p g)(\theta) = g(\theta)^\top \nabla \log p(\theta) + \nabla \cdot g(\theta), \quad (6)$$

where g is a vector-valued function and $\nabla \cdot g$ is its divergence. For an *unconstrained* domain with $\mathbb{E}_p[\|\nabla \log p(\theta)\|_2] < \infty$, Stein’s identity (5) holds for this operator whenever $g \in C^1$ is bounded and Lipschitz by [28, proof of Prop. 3]. However, on constrained domains Θ , Stein’s identity fails to hold for many reasonable inputs g if p is non-vanishing or explosive at the boundary.

Motivated by this deficiency and by a desire to exploit non-Euclidean geometry, we propose an alternative *mirrored Stein operator*,

$$(\mathcal{M}_{p,\psi} g)(\theta) = g(\theta)^\top \nabla^2\psi(\theta)^{-1}\nabla \log p(\theta) + \nabla \cdot (\nabla^2\psi(\theta)^{-1}g(\theta)), \quad (7)$$

where ψ is a strictly convex mirror function as in Sec. 2.1 with continuously differentiable $\nabla^2\psi^{-1}(\theta)$. We derive this operator from the generator of the mirror-Langevin diffusion (4) in App. C. The following result, proved in App. F.1, shows that $\mathcal{M}_{p,\psi}$ generates mean-zero functions under p whenever $\nabla^2\psi^{-1}$ suitably cancels the growth of p at the boundary.

Proposition 1. *Suppose that $\nabla^2\psi(\theta)^{-1}\nabla \log p(\theta)$ and $\nabla \cdot \nabla^2\psi(\theta)^{-1}$ are p -integrable. If $\lim_{r \rightarrow \infty} \int_{\partial\Theta_r} p(\theta)\|\nabla^2\psi(\theta)^{-1}n_r(\theta)\|_2 d\theta = 0$ for $\Theta_r \triangleq \{\theta \in \Theta : \|\theta\|_\infty \leq r\}$ and $n_r(\theta)$ the outward unit normal vector to $\partial\Theta_r$ at θ , then $\mathbb{E}_p[(\mathcal{M}_{p,\psi} g)(\theta)] = 0$ if $g \in C^1$ is bounded Lipschitz.*

Example 1 (Dirichlet p , Negative entropy ψ). When $\theta_{1:d+1} \sim \text{Dir}(\alpha)$ for $\alpha \in \mathbb{R}_+^{d+1}$, even the common identity $\mathbb{E}_p[\nabla \log p(\theta)] = 0$ need not hold when some $\alpha_j \leq 1$. However, when $\psi(\theta) = \sum_{j=1}^{d+1} \theta_j \log \theta_j$, the conditions of Prop. 1 are met for any α as $\nabla^2\psi(\theta)^{-1} = \text{diag}(\theta) - \theta\theta^\top$,

$$\begin{aligned} \int_{\partial\Theta} p(\theta)g(\theta)^\top \nabla^2\psi(\theta)^{-1}n(\theta)d\theta &= \sum_{j=1}^d \int_{\theta_j=0} p(\theta)(\theta^\top g(\theta) - g_j(\theta))\theta_j d\theta - j \\ &\quad + \frac{1}{\sqrt{d}} \int_{\theta_{d+1}=0} p(\theta)\theta^\top g(\theta)\theta_{d+1} d\theta = 0 \end{aligned}$$

¹A matrix divergence $\nabla \cdot G(\theta)$ is the vector obtained by computing the divergence of each row of $G(\theta)$.

by Ding [16, (4)] for any bounded g and $n(\theta)$ the outward unit normal vector to $\partial\Theta$ at θ , and $\lim_{r \rightarrow \infty} \int_{\partial\Theta_r} p(\theta) \|\nabla^2 \psi(\theta)^{-1} n_r(\theta)\|_2 d\theta = \sup_{\|g\|_\infty \leq 1} \int_{\partial\Theta} p(\theta) g(\theta)^\top \nabla^2 \psi(\theta)^{-1} n(\theta) d\theta$. Remarkably, the mirror-Langevin diffusion for our choice of ψ is the Wright-Fisher diffusion [20] which Gan et al. [24] recently used to bound distances to Dirichlet distributions.

4 Sampling with Mirrored Stein Operators

Liu and Wang [44] pioneered the idea of using Stein operators to approximate a target distribution with particles. Their popular SVGD algorithm deterministically updates a set of n particle locations on each step and relies on the interaction between them to approximately sample from a target distribution p . The following theorem summarizes their main findings.

Theorem 2 ([44, Thm. 3.1]). *Suppose $(\theta_t)_{t \geq 0}$ satisfies $d\theta_t = g_t(\theta_t)dt$ for bounded Lipschitz $g_t \in C^1 : \mathbb{R}^d \rightarrow \mathbb{R}^d$ and that θ_t has density q_t with $\mathbb{E}_{q_t}[\|\nabla \log q_t(\theta)\|_2] < \infty$. If $\text{KL}(q_t \| p) \triangleq \mathbb{E}_{q_t}[\log(q_t(\theta)/p(\theta))]$ exists then, for the Langevin Stein operator \mathcal{S}_p (6),*

$$\frac{d}{dt} \text{KL}(q_t \| p) = -\mathbb{E}_{q_t}[(\mathcal{S}_p g_t)(\theta)]. \quad (8)$$

To sample from a target distribution p , we aim to find the choice of update direction g_t that most quickly decreases $\text{KL}(q_t \| p)$ at time t , i.e., we aim to minimize $\frac{d}{dt} \text{KL}(q_t \| p)$ over a set \mathcal{G} of candidate directions g_t . SVGD chooses g_t in a reproducing kernel Hilbert space [RKHS, 6] norm ball $\mathcal{B}_{\mathcal{H}^d} = \{g : \|g\|_{\mathcal{H}^d} \leq 1\}$, where \mathcal{H}^d is the product RKHS containing vector-valued functions with each component in the RKHS \mathcal{H} of k . Then the optimal $g_t^* \in \mathcal{B}_{\mathcal{H}^d}$ that minimizes (8) is

$$g_t^* \propto g_{q_t, k}^* \triangleq \mathbb{E}_{q_t}[k(\theta, \cdot) \nabla \log p(\theta) + \nabla_\theta k(\theta, \cdot)] = \mathbb{E}_{q_t}[\mathcal{S}_p K_k(\cdot, \theta)],$$

where we let $K_k(\theta, \theta') = k(\theta, \theta')I$, and $\mathcal{S}_p K_k(\cdot, \theta)$ denotes applying \mathcal{S}_p to each row of $K_k(\cdot, \theta)$. SVGD has found great success in approximating unconstrained target distributions p but breaks down for constrained targets and fails to exploit non-Euclidean geometry. Our goal is to develop new particle evolution samplers suitable for constrained domains and non-Euclidean geometries.

4.1 Mirrored dynamics

SVGD encounters two difficulties when faced with a constrained support. First, the SVGD updates can push the random variable θ_t outside of its support Θ , rendering all future updates undefined. Second, Stein's identity (5) often fails to hold for candidate directions in $\mathcal{B}_{\mathcal{H}^d}$ (cf. Ex. 1). When this occurs, SVGD need not converge to p as p is not a stationary point of its dynamics (i.e., $\frac{d}{dt} \text{KL}(q_t \| p)|_{q_t=p} \neq 0$ when $q_t = p$). Inspired by mirror descent [50], we consider the following *mirrored* dynamics

$$\theta_t = \nabla \psi^*(\eta_t) \quad \text{for} \quad d\eta_t = g_t(\eta_t)dt, \quad \text{or, equivalently,} \quad d\theta_t = \nabla^2 \psi(\theta_t)^{-1} g_t(\eta_t)dt, \quad (9)$$

where $g_t : \Theta \rightarrow \mathbb{R}^d$ now represents the update direction in η space. The inverse mirror map $\nabla \psi^*$ automatically guarantees that θ_t belongs to the constrained domain Θ . From Thm. 2 it follows that

$$\frac{d}{dt} \text{KL}(q_t \| p) = -\mathbb{E}_{q_t}[(\mathcal{M}_{p, \psi} g_t)(\theta)], \quad (10)$$

where $\mathcal{M}_{p, \psi}$ is the mirrored Stein operator (7). In the following sections, we propose three new deterministic sampling algorithms by seeking the optimal direction g_t that minimizes (10) over different function classes. Thm. 3 (proved in App. F.2) forms the basis of our analysis.

Theorem 3 (Optimal mirror updates in RKHS). *Suppose $(\theta_t)_{t \geq 0}$ follows the mirrored dynamics (9). Let \mathcal{H}_K denote the RKHS of a matrix-valued kernel $K : \Theta \times \Theta \rightarrow \mathbb{S}^{d \times d}$ [49]. Then, the optimal direction of g_t that minimizes (10) in the norm ball $\mathcal{B}_{\mathcal{H}_K} \triangleq \{g : \|g\|_{\mathcal{H}_K} \leq 1\}$ is*

$$g_t^* \propto g_{q_t, K}^* \triangleq \mathbb{E}_{q_t}[\mathcal{M}_{p, \psi} K(\cdot, \theta)], \quad (11)$$

where $\mathcal{M}_{p, \psi} K(\cdot, \theta)$ applies $\mathcal{M}_{p, \psi}$ (7) to each row of the matrix-valued function $K_\theta = K(\cdot, \theta)$.

4.2 Mirrored Stein Variational Gradient Descent

Following the pattern of SVGD, one can choose the matrix-valued K of Thm. 3 to be $K_k(\theta, \theta') = k(\theta, \theta')I$, where k is any scalar-valued kernel on Θ . In this case, the resulting update $g_{q_t, K_k}^*(\cdot) = \mathbb{E}_{q_t}[\mathcal{M}_{p, \psi} K_k(\cdot, \theta)]$ is equivalent to running SVGD in the dual η space before mapping back to Θ .

Algorithm 1 Mirrored Stein Variational Gradient Descent & Stein Variational Mirror Descent

Input: density p on Θ , kernel k , mirror function ψ , particles $(\theta_0^i)_{i=1}^n \subset \Theta$, step sizes $(\epsilon_t)_{t=1}^T$
Init: $\eta_0^i \leftarrow \nabla\psi(\theta_0^i)$ for $i \in [n]$
for $t = 0 : T$ **do**
 if SVMD **then** $K_t \leftarrow K_{\psi,t}$ (14) **else** $K_t \leftarrow kI$ (MSVGD)
 for $i \in [n]$, $\eta_{t+1}^i \leftarrow \eta_t^i + \epsilon_t \frac{1}{n} \sum_{j=1}^n \mathcal{M}_{p,\psi} K_t(\theta_t^i, \theta_t^j)$ (for $\mathcal{M}_{p,\psi} K_t(\cdot, \theta)$ defined in Thm. 3)
 for $i \in [n]$, $\theta_{t+1}^i \leftarrow \nabla\psi^*(\eta_{t+1}^i)$
return $\{\theta_{T+1}^i\}_{i=1}^n$.

Theorem 4 (Mirrored SVGD updates). *In the setting of Thm. 3, let $k_{\psi}(\eta, \eta') = k(\nabla\psi^*(\eta), \nabla\psi^*(\eta'))$, $p_H(\eta) = p(\nabla\psi^*(\eta)) \cdot |\det \nabla^2\psi^*(\eta)|$ denote the density of $\eta = \nabla\psi(\theta)$ when $\theta \sim p$, and $q_{t,H}(\eta)$ denote the density of η_t under the mirrored dynamics (9). If $K_k = kI$,*

$$g_{q_t, K_k}^*(\theta_t) = \mathbb{E}_{q_{t,H}}[k_{\psi}(\eta, \eta_t) \nabla \log p_H(\eta) + \nabla_{\eta} k_{\psi}(\eta, \eta_t)]. \quad (12)$$

The proof is in App. F.3. By discretizing the dynamics $d\eta_t = g_{q_t, K_k}^*(\theta_t) dt$ and initializing with any particle approximation $q_0 = \frac{1}{n} \sum_{i=1}^n \delta_{\theta_0^i}$, we obtain *Mirrored SVGD (MSVGD)*, our first algorithm for sampling in constrained domains. The details are summarized in Alg. 1.

When only a single particle is used ($n = 1$) and the differentiable input kernel satisfies $\nabla k(\theta, \theta) = 0$, the MSVGD update (12) reduces to gradient descent on $-\log p_H(\eta)$. Note however that the modes of the mirrored density $p_H(\eta)$ need not match those of the target density $p(\theta)$. Since we are primarily interested in the θ -space density, it is natural to ask whether there exists a mirrored dynamics that reduces to finding the mode of $p(\theta)$ in this limiting case. In the next section, we give an answer to this question by designing an adaptive reproducing kernel that yields a mirror descent-like update.

4.3 Stein Variational Mirror Descent

Our second sampling algorithm for constrained problems is called *Stein Variational Mirror Descent (SVMD)*. We start by introducing a new matrix-valued kernel that incorporates the metric $\nabla^2\psi$ and evolves with the distribution q_t .

Definition 1 (Kernels for SVMD). *Given a continuous scalar-valued kernel k , consider the Mercer representation² $k(\theta, \theta') = \sum_{i \geq 1} \lambda_i u_i(\theta) u_i(\theta')$ w.r.t. q_t , where u_i is an eigenfunction satisfying*

$$\mathbb{E}_{q_t(\theta')} [k(\theta, \theta') u_i(\theta')] = \lambda_i u_i(\theta). \quad (13)$$

For $k^{1/2}(\theta, \theta') \triangleq \sum_{i \geq 1} \lambda_i^{1/2} u_i(\theta) u_i(\theta')$, we define the adaptive SVMD kernel at time t ,

$$K_{\psi,t}(\theta, \theta') \triangleq \mathbb{E}_{\theta_t \sim q_t} [k^{1/2}(\theta, \theta_t) \nabla^2\psi(\theta_t) k^{1/2}(\theta_t, \theta')]. \quad (14)$$

By Thm. 3, the optimal update direction for the SVMD kernel ball is $g_{q_t, K_{\psi,t}}^* = \mathbb{E}_{q_t} [\mathcal{M}_{p,\psi} K_{\psi,t}(\cdot, \theta)]$. We obtain the SVMD algorithm (summarized in Alg. 1) by discretizing $d\eta_t = g_{q_t, K_{\psi,t}}^*(\theta_t) dt$ and initializing with $q_0 = \frac{1}{n} \sum_{i=1}^n \delta_{\theta_0^i}$. Because of the discrete representation of q_t , $K_{\psi,t}$ takes the form

$$K_{\psi,t}(\theta, \theta') = \sum_{i=1}^n \sum_{j=1}^n \lambda_i^{1/2} \lambda_j^{1/2} u_i(\theta) u_j(\theta') \Gamma_{ij}, \text{ for } \Gamma_{ij} = \frac{1}{n} \sum_{\ell=1}^n u_i(\theta_t^\ell) u_j(\theta_t^\ell) \nabla^2\psi(\theta_t^\ell).$$

Here both λ_i and $u_i(\theta^j)$ can be computed by solving a matrix eigenvalue problem involving the particle set $\{\theta^i\}_{i=1}^n$: $Bv_j = n\lambda_j v_j$, where $B = (k(\theta^i, \theta^j))_{i,j=1}^n \in \mathbb{R}^{n \times n}$ is the Gram matrix of pairwise kernel evaluations at particle locations, and the i -th element of v_j is $u_j(\theta^i)$. To compute $\nabla_{\theta} K_{\psi,t}(\theta, \theta')$, we differentiate both sides of (13) to find that $\nabla u_j(\theta^i) = \frac{1}{\lambda_j} \sum_{\ell=1}^n v_{j\ell} \nabla_{\theta^i} k(\theta^i, \theta^\ell)$. This technique was used in [58] to estimate gradients of eigenfunctions w.r.t. a continuous q . Following their recommendations, we truncate the sum at the J -th largest eigenvalues according to a threshold ($\tau = \sum_{j=1}^J \lambda_j / \sum_{j=1}^n \lambda_j$) to ensure numerical stability.

Notably, SVMD differs from MSVGD only in its choice of kernel, but, whenever $\nabla k(\theta, \theta) = 0$, this change is sufficient to exactly recover mirror descent when $n = 1$.

²See App. D for background on Mercer representations in non-compact domains.

Proposition 5 (Single-particle SVMD is mirror descent). *If $n = 1$, then one step of SVMD becomes*

$$\eta_{t+1} = \eta_t + \epsilon_t(k(\theta_t, \theta_t)\nabla \log p(\theta_t) + \nabla k(\theta_t, \theta_t)), \quad \theta_{t+1} = \nabla\psi^*(\eta_{t+1}).$$

Proof When $n = 1$, $\lambda_1 = k(\theta_t, \theta_t)$, $u_1 = 1$, and thus $K_{\psi,t}(\theta_t, \theta_t) = k(\theta_t, \theta_t)\nabla^2\psi(\theta_t)$. \square

4.4 Stein Variational Natural Gradient

The fact that SVMD recovers mirror descent as a special case is not only of relevance in constrained problems. We next exploit the connection between MD and natural gradient descent discussed in Sec. 2.1 to design a new sampler – *Stein Variational Natural Gradient (SVNG)* – that more efficiently approximates unconstrained targets. The idea is to replace the Hessian $\nabla^2\psi(\cdot)$ in the SVMD dynamics $d\theta_t = \nabla^2\psi(\theta_t)^{-1}g_{q_t, K_{\psi,t}}^*(\theta_t)$ with a general metric tensor $G(\cdot)$. The result is the Riemannian gradient flow

$$d\theta_t = G(\theta_t)^{-1}g_{q_t, K_{G,t}}^*(\theta_t)dt \quad \text{with} \quad K_{G,t}(\theta, \theta') \triangleq \mathbb{E}_{\theta_t \sim q_t}[k^{1/2}(\theta, \theta_t)G(\theta_t)k^{1/2}(\theta_t, \theta')]. \quad (15)$$

Given any initial particle approximation $q_0 = \frac{1}{n} \sum_{i=1}^n \delta_{\theta_0^i}$, we discretize these dynamics to obtain the unconstrained SVNG sampler of Alg. 2 in the appendix. SVNG can be seen as an instance of MatSVGD [66] with a new adaptive time-dependent kernel $G^{-1}(\theta)K_{G,t}(\theta, \theta')G^{-1}(\theta')$. However, similar to Prop. 5 and unlike the heuristic kernels of [66], SVNG reduces to natural gradient ascent for finding the mode of $p(\theta)$ when $n = 1$. SVNG is well-suited to Bayesian inference problems where the target is a posterior distribution $p(\theta) \propto \pi(\theta)\pi(y|\theta)$. There, the metric tensor $G(\theta)$ can be set to the Fisher information matrix $\mathbb{E}_{\pi(y|\theta)}[\nabla \log \pi(y|\theta)\nabla \log \pi(y|\theta)^\top]$ of the data likelihood $\pi(y|\theta)$. Ample precedent from natural gradient variational inference [33, 38] and Riemannian MCMC [53] suggests that encoding problem geometry in this manner often leads to more rapid convergence.

5 Experiments

We next conduct a series of simulated and real-data experiments to assess (1) distributional approximation on the simplex, (2) frequentist confidence interval construction for (constrained) post-selection inference, and (3) large-scale posterior inference with non-Euclidean geometry. To compare with standard SVGD on constrained domains and to prevent its particles from exiting the domain Θ , we introduce a Euclidean projection onto Θ following each SVGD update. See App. E for supplementary experimental details and <https://github.com/thjashin/mirror-stein-samplers> for Python and R code replicating all experiments.

5.1 Approximation quality on the simplex

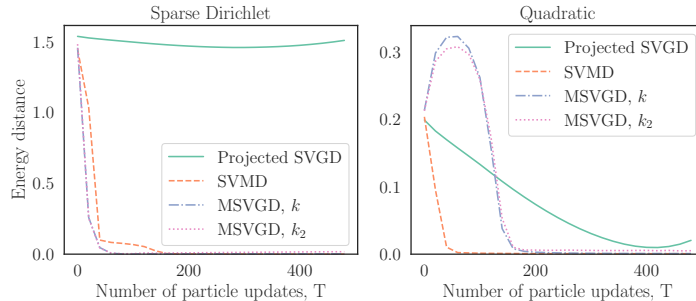


Figure 2: Quality of 50-particle approximations to 20-dimensional distributions on the simplex after T particle updates. (Left) Sparse Dirichlet posterior of [53]. (Right) Quadratic simplex target of [1].

We first measure distributional approximation quality using two 20-dimensional simplex-constrained targets from the literature: the sparse Dirichlet posterior of [53] extended to 20 dimensions and the quadratic simplex target of [1]. The Dirichlet target mimics the multimodal sparse conditionals that arise in latent Dirichlet allocation [8] but induces a log concave distribution in η space, while the

quadratic is log-concave in θ space. In Fig. 2, we compare the quality of MSVGD, SVMD, and projected SVGD with $n = 50$ particles and inverse multiquadric base kernel k [27] by computing the energy distance [61] to a surrogate ground truth sample of size 1000 (drawn i.i.d. or, in the quadratic case, from the No-U-Turn Sampler [32]). We also compare to MSVGD with $k_2(\theta, \theta') = k(\nabla\psi(\theta), \nabla\psi(\theta'))$, a choice which corresponds to running SVGD in the dual space with kernel k by Thm. 4 and which ensures the convergence of MSVGD to p by the upcoming Thms. 6 to 8.

In the quadratic case, SVMD is favored over MSVGD as it is able to exploit the log-concavity of $p(\theta)$. In contrast, for the multimodal sparse Dirichlet with $p(\theta)$ unbounded near the boundary, MSVGD converges slightly more rapidly than SVMD by exploiting the log concave structure in η space. This parallels the observation of [34] that LMC in the mirror space outperforms Riemannian LMC for sparse Dirichlet distributions. Projected SVGD fails to converge to the target in both cases and has particular difficulty in approximating the sparse Dirichlet target with unbounded density. MSVGD with k and k_2 perform very similarly, but we observe that k yields better approximation quality upon convergence. Therefore, we employ k in the remaining MSVGD experiments.

5.2 Confidence intervals for post-selection inference

We next apply our algorithms to the constrained sampling problems that arise in post-selection inference [62, 40]. Specifically, we consider the task of forming valid confidence intervals (CIs) for regression parameters selected using the randomized Lasso [63] with data $X \in \mathbb{R}^{\tilde{n} \times p}$ and $y \in \mathbb{R}^{\tilde{n}}$ and user-generated randomness $w \in \mathbb{R}^p$ from a log-concave distribution with density g . The randomized Lasso returns $\hat{\beta} \in \mathbb{R}^p$ with non-zero coefficients denoted by $\hat{\beta}_E$ and their signs by s_E . It is common practice to report least squares CIs for β_E by running a linear regression on the selected features E . However, since E is chosen based on the same data, the resulting CIs are often invalid.

Post-selection inference solves this problem by conditioning the inference on the knowledge of E and s_E . To construct valid CIs, it suffices to approximate the *selective distribution* with support $\{\hat{\beta}_E, u_{-E} : s_E \odot \hat{\beta}_E > 0, u_{-E} \in [-1, 1]^{p-|E|}\}$ and density

$$\hat{g}(\hat{\beta}_E, u_{-E}) \propto g\left(X^\top y - \begin{pmatrix} X_E^\top X_E + \epsilon I_{|E|} \\ X_{-E}^\top X_E \end{pmatrix} \hat{\beta}_E + \lambda \begin{pmatrix} s_E \\ u_{-E} \end{pmatrix}\right).$$

In our experiments, we integrate out u_{-E} analytically, following [63], and model $|\hat{\beta}_E|$ rather than $\hat{\beta}_E$ to obtain a log-concave density supported on the positive orthant with mirror function $\psi(\theta) = \sum_{j=1}^d (\theta_j \log \theta_j - \theta_j)$. In Fig. 4a we show the example of a 2D selective distribution using samples drawn by NUTS [32]. We also plot the results by projected SVGD, SVMD, and MSVGD in this example. Projected SVGD fails to approximate the target with many samples gathering at the truncation boundary, while the samples by MSVGD and SVMD closely resemble the truth.

We then compare our methods with the standard `norejection` MCMC approach of the `selectiveInference` R package [64] using the example simulation setting described in [57] and a penalty factor 0.7. To generate N total sample points we run MCMC for N iterations after burn-in or aggregate the particles from N/n independent runs of MSVGD or SVMD with $n = 50$ particles. As N ranges from 1000 to 3000 in Fig. 3a, the MSVGD and SVMD CIs consistently yield higher coverage than the standard 90% CIs. This increased coverage is of particular value for smaller sample sizes, for which the standard CIs tend to undercover. For a much larger sample size of $N = 5000$ in Fig. 3b, the SVMD and standard CIs closely track one another across confidence levels, while MSVGD consistently yields longer CIs with high coverage. The higher coverage of MSVGD is only of value for larger confidence levels at which the other methods begin to undercover.

We next apply our samplers to a post-selection inference task on the HIV-1 drug resistance dataset [55], where we run randomized Lasso [63] to find statistically significant mutations associated with drug resistance using susceptibility data on virus isolates. We take the *vitro* measurement of log-fold change under the 3TC drug as response and include mutations that had appeared at least 11 times in the dataset as regressors. In Fig. 4b we plot the CIs of selected mutations obtained with $N = 5000$ sample points. We see that the invalid unadjusted least squares CIs can lead to premature conclusions, e.g., declaring mutation 215Y significant when there is insufficient support after conditioning on the selection event. In contrast, mutation 184V, which has known association with drug resistance, is declared significant by all methods even after post-selection adjustment. The MSVGD and SVMD CIs mostly track those of the standard `selectiveInference` method, but their conclusions sometimes differ: e.g., 62Y is flagged as significant by MSVGD and SVMD but not by `selectiveInference`.

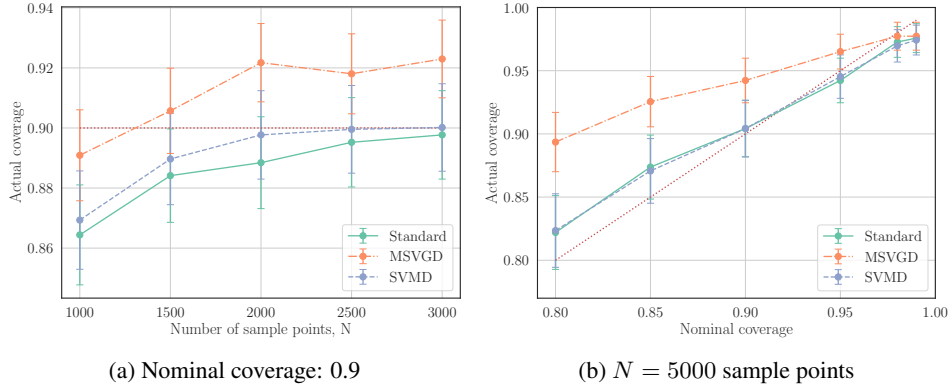


Figure 3: Coverage of post-selection CIs across (a) 500 / (b) 200 replications of simulation of [57].

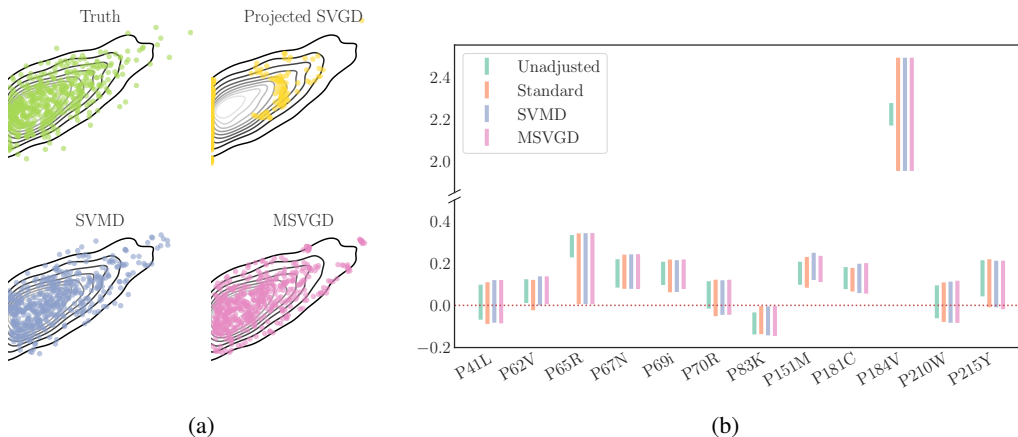


Figure 4: (a) Sampling from a 2D selective density; (b) Unadjusted and post-selection CIs for the mutations selected by the randomized Lasso as candidates for HIV-1 drug resistance (see Sec. 5.2).

5.3 Large-scale posterior inference with non-Euclidean geometry

Finally, we demonstrate the advantages of exploiting non-Euclidean geometry by recreating the real-data large-scale Bayesian logistic regression experiment of [44] with 581,012 datapoints and $d = 54$ feature dimensions. Here, the target p is the posterior distribution over logistic regression parameters. We adopt the Fisher information metric tensor G , compare 20-particle SVND to SVGD and its prior geometry-aware variants RSVG [42] and MatSVG [66], and for all methods use stochastic minibatches of size 256 to scalably approximate each log likelihood query. In Fig. 5, all geometry-aware methods substantially improve the log predictive probability of SVGD.³ SVNG also strongly outperforms RSVG and converges to its maximum test probability in half as many steps as MatSVG (Avg) and more rapidly than MatSVG (Mixture).

6 Convergence Guarantees

We next turn our attention to the convergence properties of our proposed methods. For K_t and ϵ_t as in Alg. 1, let $(q_t^\infty, q_{t,H}^\infty)$ represent the distributions of the mirrored Stein updates (θ_t, η_t) when $\theta_0 \sim q_0^\infty$ and $\eta_{t+1} = \eta_t + \epsilon_t g_{q_t, K_t}^*(\theta_t)$ for $t \geq 0$. Our first result, proved in App. F.4, shows that if the Alg. 1 initialization $q_{0,H}^n = \frac{1}{n} \sum_{i=1}^n \delta_{\eta_0^i}$ converges in Wasserstein distance to a distribution $q_{0,H}^\infty$ as $n \rightarrow \infty$, then, on each round $t > 0$, the output of Alg. 1, $q_t^n = \frac{1}{n} \sum_{i=1}^n \delta_{\theta_t^i}$, converges to q_t^∞ .

³Notably, on the same dataset, SVGD was shown to outperform preconditioned stochastic gradient Langevin dynamics [41], a leading MCMC method imbued with geometric information [66].

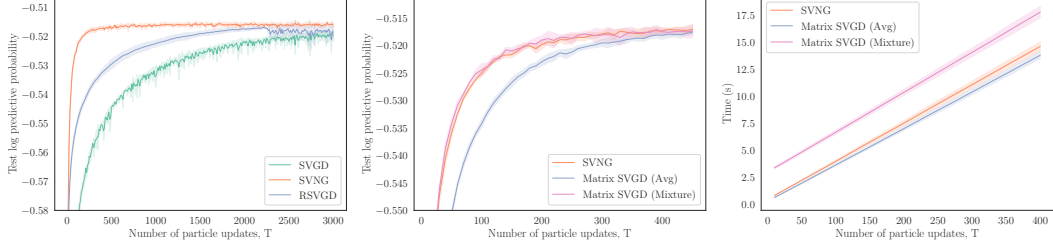


Figure 5: Value of non-Euclidean geometry in large-scale Bayesian logistic regression.

Theorem 6 (Convergence of mirrored updates as $n \rightarrow \infty$). *Suppose Alg. 1 is initialized with $q_{0,H}^n = \frac{1}{n} \sum_{i=1}^n \delta_{\eta_0^i}$ satisfying $W_1(q_{0,H}^n, q_{0,H}^\infty) \rightarrow 0$ for W_1 the L^1 Wasserstein distance. Define the η -induced kernel $K_{\nabla\psi^*,t}(\eta, \eta') \triangleq K_t(\nabla\psi^*(\eta), \nabla\psi^*(\eta'))$. If, for some $c_1, c_2 > 0$,*

$$\begin{aligned} \|\nabla(K_{\nabla\psi^*,t}(\cdot, \eta)\nabla\log p_H(\eta) + \nabla \cdot K_{\nabla\psi^*,t}(\cdot, \eta))\|_{\text{op}} &\leq c_1(1 + \|\eta\|_2), \\ \|\nabla(K_{\nabla\psi^*,t}(\eta', \cdot)\nabla\log p_H(\cdot) + \nabla \cdot K_{\nabla\psi^*,t}(\eta', \cdot))\|_{\text{op}} &\leq c_2(1 + \|\eta'\|_2), \end{aligned}$$

then, $W_1(q_{t,H}^n, q_{t,H}^\infty) \rightarrow 0$ and $q_t^n \Rightarrow q_t^\infty$ for each round t .

Remark The pre-conditions hold, for example, whenever $\nabla\log p_H$ is Lipschitz, ψ is strongly convex, and $K_t = kI$ for k bounded with bounded derivatives.

Given a mirrored Stein operator (7), an arbitrary Stein set \mathcal{G} , and an arbitrary matrix-valued kernel K we define the *mirrored Stein discrepancy* and *mirrored kernel Stein discrepancy*

$$\text{MSD}(q, p, \mathcal{G}) \triangleq \sup_{g \in \mathcal{G}} \mathbb{E}_q[(\mathcal{M}_{p,\psi}g)(\theta)] \quad \text{and} \quad \text{MKSD}_K(q, p) \triangleq \text{MSD}(q, p, \mathcal{B}_{\mathcal{H}_K}). \quad (16)$$

The former is an example of a diffusion Stein discrepancy [28] and the latter an example of a diffusion kernel Stein discrepancy [4]. Since the MKSD optimization problem (16) matches that in Thm. 3, we have that $\text{MKSD}_K(q, p) = \|g_{q,K}^*\|_{\mathcal{H}_K}$. Our next result, proved in App. F.5, shows that the infinite-particle mirrored Stein updates reduce the KL divergence to p whenever the step size is sufficiently small and drive MKSD to 0 if, for example, $\epsilon_t = \Omega(\text{MKSD}_{K_t}(q_t^\infty, p)^\alpha)$ for any $\alpha > 0$.

Theorem 7 (Infinite-particle mirrored Stein updates decrease KL and MKSD). *Assume $\kappa_1 \triangleq \sup_\theta \|K_t(\theta, \theta)\|_{\text{op}} < \infty$, and $\kappa_2 \triangleq \sum_{i=1}^d \sup_\theta \|\nabla_{i,d+i}^2 K_t(\theta, \theta)\|_{\text{op}} < \infty$, $\nabla\log p_H$ is L -Lipschitz, and ψ is α -strongly convex. If $\epsilon_t < 1/(\|\nabla_{\eta_t} g_{q_t^\infty, K_t}^*(\theta_t) + \nabla_{\eta_t} g_{q_t^\infty, K_t}^*(\theta_t)^\top\|_{\text{op}})$, then*

$$\text{KL}(q_{t+1}^\infty \| p) - \text{KL}(q_t^\infty \| p) \leq -\left(\epsilon_t - \left(\frac{L\kappa_1}{2} + \frac{2\kappa_2}{\alpha^2}\right)\epsilon_t^2\right)\text{MKSD}_{K_t}(q_t^\infty, p)^2.$$

Our last result, proved in App. F.6, shows that $q_t^\infty \Rightarrow p$ if $\text{MKSD}_{K_k}(q_t^\infty, p) \rightarrow 0$. Hence, by Thms. 6 and 7, n -particle MSVGD converges weakly to p if ϵ_t decays at a suitable rate.

Theorem 8 (MKSD_{K_k} determines weak convergence). *Assume p_H is distantly dissipative [19] with $\nabla\log p_H$ Lipschitz, ψ is strictly convex with continuous $\nabla\psi^*$, and $k(\theta, \theta') = \kappa(\nabla\psi(\theta), \nabla\psi(\theta'))$ for $\kappa(x, y) = (c^2 + \|x - y\|_2^2)^\beta$ with $\beta \in (-1, 0)$. Then, $q_t^\infty \Rightarrow p$ if $\text{MKSD}_{K_k}(q_t^\infty, p) \rightarrow 0$.*

Remark The pre-conditions hold, for example, for any Dirichlet target with negative entropy ψ .

7 Discussion

This paper introduced the mirrored Stein operator along with three new particle evolution algorithms for sampling with constrained domains and non-Euclidean geometries. The first algorithm MSVGD performs SVGD updates in a mirrored space before mapping to the target domain. The other two algorithms are different discretizations of the same continuous dynamics for exploiting non-Euclidean geometry. SVMG is a multi-particle generalization of mirror descent for constrained domains, while SVNG is designed for unconstrained problems with informative metric tensors. We do not anticipate negative societal impact from this work, but we highlight three limitations. First, like SVGD, our MSVGD require n^2 time per update, and parallelism or low-rank kernel approximation may be

needed to reduce this complexity. Second, SVMD and SVNG are more costly than MSVGD due to the adaptive kernel construction. Third, we leave open the question of convergence when stochastic gradient estimates are employed, but we suspect the results of [29, Thm. 7] can be extended to our setting. In the future, we hope to deploy our mirrored Stein operators for other inferential tasks on constrained domains including sample quality measurement [26, 27, 28, 35], goodness-of-fit testing [13, 45, 36], graphical model inference [71, 65], parameter estimation [4], thinning [56], and de novo sampling [10, 11, 23].

References

- [1] Kwangjun Ahn and Sinho Chewi. Efficient constrained sampling via the mirror-Langevin algorithm. *arXiv preprint arXiv:2010.16212*, 2020.
- [2] Shun-Ichi Amari. Natural gradient works efficiently in learning. *Neural Computation*, 10(2):251–276, 1998.
- [3] Andrew D Barbour. Stein’s method and Poisson process convergence. *Journal of Applied Probability*, pages 175–184, 1988.
- [4] Alessandro Barp, Francois-Xavier Briol, Andrew Duncan, Mark Girolami, and Lester Mackey. Minimum Stein discrepancy estimators. In *Advances in Neural Information Processing Systems*, pages 12964–12976, 2019.
- [5] Amir Beck and Marc Teboulle. Mirror descent and nonlinear projected subgradient methods for convex optimization. *Operations Research Letters*, 31(3):167–175, 2003.
- [6] Alain Berlinet and Christine Thomas-Agnan. *Reproducing kernel Hilbert spaces in probability and statistics*. Springer Science & Business Media, 2011.
- [7] Rabi N Bhattacharya and Edward C Waymire. *Stochastic processes with applications*. SIAM, 2009.
- [8] David M Blei, Andrew Y Ng, and Michael I Jordan. Latent Dirichlet allocation. *Journal of Machine Learning Research*, 3:993–1022, 2003.
- [9] Peng Chen, Keyi Wu, Joshua Chen, Tom O’Leary-Roseberry, and Omar Ghattas. Projected Stein variational Newton: A fast and scalable Bayesian inference method in high dimensions. In *Advances in Neural Information Processing Systems*, volume 32, 2019.
- [10] Wilson Ye Chen, Lester Mackey, Jackson Gorham, François-Xavier Briol, and Chris Oates. Stein points. In *International Conference on Machine Learning*, pages 844–853, 2018.
- [11] Wilson Ye Chen, Alessandro Barp, François-Xavier Briol, Jackson Gorham, Mark Girolami, Lester Mackey, and Chris Oates. Stein point Markov chain Monte Carlo. In *International Conference on Machine Learning*, pages 1011–1021, 2019.
- [12] Sinho Chewi, Thibaut Le Gouic, Chen Lu, Tyler Maunu, Philippe Rigollet, and Austin Stromme. Exponential ergodicity of mirror-Langevin diffusions. *arXiv preprint arXiv:2005.09669*, 2020.
- [13] Kacper Chwialkowski, Heiko Strathmann, and Arthur Gretton. A kernel test of goodness of fit. In *International Conference on Machine Learning*, pages 2606–2615, 2016.
- [14] Arnak Dalalyan. Further and stronger analogy between sampling and optimization: Langevin Monte Carlo and gradient descent. In *Conference on Learning Theory*, pages 678–689, 2017.
- [15] Gianluca Detommaso, Tiangang Cui, Youssef Marzouk, Alessio Spantini, and Robert Scheichl. A Stein variational Newton method. In *Advances in Neural Information Processing Systems*, volume 31, pages 9187–9197, 2018.
- [16] Yiren Ding. The law of cosines for an n-dimensional simplex. *International Journal of Mathematical Education in Science and Technology*, 39(3):407–410, 2008.
- [17] John Duchi, Elad Hazan, and Yoram Singer. Adaptive subgradient methods for online learning and stochastic optimization. *Journal of Machine Learning Research*, 12(7), 2011.
- [18] Alain Durmus, Eric Moulines, and Marcelo Pereyra. Efficient Bayesian computation by proximal Markov chain Monte Carlo: when Langevin meets Moreau. *SIAM Journal on Imaging Sciences*, 11(1):473–506, 2018.
- [19] Andreas Eberle. Reflection couplings and contraction rates for diffusions. *Probability Theory and Related Fields*, 166(3):851–886, 2016.
- [20] Stewart N Ethier. A class of degenerate diffusion processes occurring in population genetics. *Communications on Pure and Applied Mathematics*, 29(5):483–493, 1976.
- [21] Yihao Feng, Dilin Wang, and Qiang Liu. Learning to draw samples with amortized Stein variational gradient descent. *Uncertainty in Artificial Intelligence*, 2017.

- [22] JC Ferreira and VA Menegatto. Eigenvalues of integral operators defined by smooth positive definite kernels. *Integral Equations and Operator Theory*, 64(1):61–81, 2009.
- [23] Futoshi Futami, Zhenghang Cui, Issei Sato, and Masashi Sugiyama. Bayesian posterior approximation via greedy particle optimization. In *Proceedings of the AAAI Conference on Artificial Intelligence*, volume 33, pages 3606–3613, 2019.
- [24] Han L Gan, Adrian Röllin, and Nathan Ross. Dirichlet approximation of equilibrium distributions in Cannings models with mutation. *Advances in Applied Probability*, 49(3):927–959, 2017.
- [25] Damien Garreau, Wittawat Jitkrittum, and Motonobu Kanagawa. Large sample analysis of the median heuristic. *arXiv preprint arXiv:1707.07269*, 2017.
- [26] Jackson Gorham and Lester Mackey. Measuring sample quality with Stein’s method. In *Advances in Neural Information Processing Systems*, pages 226–234, 2015.
- [27] Jackson Gorham and Lester Mackey. Measuring sample quality with kernels. In *International Conference on Machine Learning*, pages 1292–1301, 2017.
- [28] Jackson Gorham, Andrew B Duncan, Sebastian J Vollmer, and Lester Mackey. Measuring sample quality with diffusions. *The Annals of Applied Probability*, 29(5):2884–2928, 2019.
- [29] Jackson Gorham, Anant Raj, and Lester Mackey. Stochastic stein discrepancies. *arXiv preprint arXiv:2007.02857*, 2020.
- [30] Tuomas Haarnoja, Haoran Tang, Pieter Abbeel, and Sergey Levine. Reinforcement learning with deep energy-based policies. In *International Conference on Machine Learning*, pages 1352–1361, 2017.
- [31] Geoffrey Hinton, Nitish Srivastava, and Kevin Swersky. Neural networks for machine learning lecture 6a: overview of mini-batch gradient descent. 2012.
- [32] Matthew D Hoffman and Andrew Gelman. The No-U-Turn sampler: adaptively setting path lengths in Hamiltonian Monte Carlo. *Journal of Machine Learning Research*, 15(1):1593–1623, 2014.
- [33] Matthew D Hoffman, David M Blei, Chong Wang, and John Paisley. Stochastic variational inference. *Journal of Machine Learning Research*, 14(5), 2013.
- [34] Ya-Ping Hsieh, Ali Kavis, Paul Rolland, and Volkan Cevher. Mirrored Langevin dynamics. In *Advances in Neural Information Processing Systems*, pages 2878–2887, 2018.
- [35] Jonathan Huggins and Lester Mackey. Random feature Stein discrepancies. In S. Bengio, H. Wallach, H. Larochelle, K. Grauman, N. Cesa-Bianchi, and R. Garnett, editors, *Advances in Neural Information Processing Systems*, pages 1903–1913. 2018.
- [36] Wittawat Jitkrittum, Wenkai Xu, Zoltán Szabó, K. Fukumizu, and A. Gretton. A Linear-Time Kernel Goodness-of-Fit Test. In *Advances in Neural Information Processing Systems*, 2017.
- [37] Sham Kakade, Shai Shalev-Shwartz, Ambuj Tewari, et al. On the duality of strong convexity and strong smoothness: Learning applications and matrix regularization. *Unpublished Manuscript*, 2(1), 2009.
- [38] Mohammad Emtiyaz Khan and Didrik Nielsen. Fast yet simple natural-gradient descent for variational inference in complex models. In *2018 International Symposium on Information Theory and Its Applications (ISITA)*, pages 31–35. IEEE, 2018.
- [39] Taesup Kim, Jaesik Yoon, Ousmane Dia, Sungwoong Kim, Yoshua Bengio, and Sungjin Ahn. Bayesian model-agnostic meta-learning. *Advances in Neural Information Processing Systems*, 2018.
- [40] Jason D Lee, Dennis L Sun, Yuekai Sun, and Jonathan E Taylor. Exact post-selection inference, with application to the lasso. *Annals of Statistics*, 44(3):907–927, 2016.
- [41] Chunyuan Li, Changyou Chen, David Carlson, and Lawrence Carin. Preconditioned stochastic gradient langevin dynamics for deep neural networks. In *Proceedings of the AAAI Conference on Artificial Intelligence*, volume 30, 2016.
- [42] Chang Liu and Jun Zhu. Riemannian Stein variational gradient descent for Bayesian inference. In *Proceedings of the AAAI Conference on Artificial Intelligence*, pages 3627–3634, 2018.
- [43] Qiang Liu. Stein variational gradient descent as gradient flow. In *Advances in Neural Information Processing Systems*, pages 3115–3123, 2017.
- [44] Qiang Liu and Dilin Wang. Stein variational gradient descent: A general purpose Bayesian inference algorithm. *Advances in Neural Information Processing Systems*, 29:2378–2386, 2016.
- [45] Qiang Liu, Jason Lee, and Michael Jordan. A kernelized Stein discrepancy for goodness-of-fit tests. In *International Conference on Machine Learning*, pages 276–284, 2016.
- [46] Yi-An Ma, Tianqi Chen, and Emily Fox. A complete recipe for stochastic gradient MCMC. In *Advances in Neural Information Processing Systems*, pages 2917–2925, 2015.

- [47] Yi-An Ma, Niladri Chatterji, Xiang Cheng, Nicolas Flammarion, Peter Bartlett, and Michael I Jordan. Is there an analog of Nesterov acceleration for MCMC? *arXiv preprint arXiv:1902.00996*, 2019.
- [48] James Martens. New insights and perspectives on the natural gradient method. *arXiv preprint arXiv:1412.1193*, 2014.
- [49] Charles A Micchelli and Massimiliano Pontil. On learning vector-valued functions. *Neural Computation*, 17(1):177–204, 2005.
- [50] Arkadij Semenovic Nemirovskij and David Borisovich Yudin. Problem complexity and method efficiency in optimization. 1983.
- [51] Chris J Oates, Mark Girolami, and Nicolas Chopin. Control functionals for Monte Carlo integration. *Journal of the Royal Statistical Society: Series B (Methodological)*, 79(3):695–718, 2017.
- [52] Bernt Øksendal. *Stochastic Differential Equations: An Introduction with Applications*. Springer Science & Business Media, 2003.
- [53] Sam Patterson and Yee Whye Teh. Stochastic gradient Riemannian Langevin dynamics on the probability simplex. In *Advances in Neural Information Processing Systems*, pages 3102–3110, 2013.
- [54] Garvesh Raskutti and Sayan Mukherjee. The information geometry of mirror descent. *IEEE Transactions on Information Theory*, 61(3):1451–1457, 2015.
- [55] Soo-Yon Rhee, Jonathan Taylor, Gauhar Wadhera, Asa Ben-Hur, Douglas L Brutlag, and Robert W Shafer. Genotypic predictors of human immunodeficiency virus type 1 drug resistance. *Proceedings of the National Academy of Sciences*, 103(46):17355–17360, 2006.
- [56] Marina Riabiz, Wilson Chen, Jon Cockayne, Pawel Swietach, Steven A Niederer, Lester Mackey, Chris Oates, et al. Optimal thinning of MCMC output. *arXiv preprint arXiv:2005.03952*, 2020.
- [57] Amir Sepehri and Jelena Markovic. Non-reversible, tuning-and rejection-free Markov chain Monte Carlo via iterated random functions. *arXiv preprint arXiv:1711.07177*, 2017.
- [58] Jiaxin Shi, Shengyang Sun, and Jun Zhu. A spectral approach to gradient estimation for implicit distributions. In *International Conference on Machine Learning*, pages 4644–4653, 2018.
- [59] Umut Simsekli, Roland Badeau, Taylan Cemgil, and Gaël Richard. Stochastic quasi-Newton Langevin Monte Carlo. In *International Conference on Machine Learning*, pages 642–651, 2016.
- [60] Charles Stein. A bound for the error in the normal approximation to the distribution of a sum of dependent random variables. In *Proceedings of the Sixth Berkeley Symposium on Mathematical Statistics and Probability, Volume 2: Probability Theory*. The Regents of the University of California, 1972.
- [61] Gábor J Székely and Maria L Rizzo. Energy statistics: A class of statistics based on distances. *Journal of Statistical Planning and Inference*, 143(8):1249–1272, 2013.
- [62] Jonathan Taylor and Robert J Tibshirani. Statistical learning and selective inference. *Proceedings of the National Academy of Sciences*, 112(25):7629–7634, 2015.
- [63] Xiaoying Tian and Jonathan Taylor. Selective inference with a randomized response. *The Annals of Statistics*, 46(2):679–710, 2018.
- [64] Ryan Tibshirani, Rob Tibshirani, Jonatha Taylor, Joshua Loftus, Stephen Reid, and Jelena Markovic. *selectiveInference: Tools for Post-Selection Inference*, 2019. URL <https://CRAN.R-project.org/package=selectiveInference>. R package version 1.2.5.
- [65] Dilin Wang, Zhe Zeng, and Qiang Liu. Stein variational message passing for continuous graphical models. In *International Conference on Machine Learning*, pages 5219–5227, 2018.
- [66] Dilin Wang, Ziyang Tang, Chandrajit Bajaj, and Qiang Liu. Stein variational gradient descent with matrix-valued kernels. In *Advances in Neural Information Processing Systems*, pages 7836–7846, 2019.
- [67] Max Welling and Yee W Teh. Bayesian learning via stochastic gradient Langevin dynamics. In *International Conference on Machine Learning*, pages 681–688, 2011.
- [68] Edwin B Wilson. Probable inference, the law of succession, and statistical inference. *Journal of the American Statistical Association*, 22(158):209–212, 1927.
- [69] Tatiana Xifara, Chris Sherlock, Samuel Livingstone, Simon Byrne, and Mark Girolami. Langevin diffusions and the Metropolis-adjusted Langevin algorithm. *Statistics & Probability Letters*, 91:14–19, 2014.
- [70] Kelvin Shuangjian Zhang, Gabriel Peyré, Jalal Fadili, and Marcelo Pereyra. Wasserstein control of mirror Langevin Monte Carlo. *arXiv preprint arXiv:2002.04363*, 2020.
- [71] Jingwei Zhuo, Chang Liu, Jiaxin Shi, Jun Zhu, Ning Chen, and Bo Zhang. Message passing Stein variational gradient descent. In *International Conference on Machine Learning*, pages 6018–6027, 2018.

Algorithm 2 Stein Variational Natural Gradient (SVNG)

Input: density $p(\theta)$ on \mathbb{R}^d , kernel k , metric tensor $G(\theta)$, particles $(\theta_0^i)_{i=1}^n$, step sizes $(\epsilon_t)_{t=1}^T$
for $t = 0 : T$ **do**
 for $i \in [n]$, $\theta_{t+1}^i \leftarrow \theta_t^i + \epsilon_t G(\theta_t^i)^{-1} g_{G,t}^*(\theta_t^i)$, where
 $g_{G,t}^*(\theta) = \frac{1}{n} \sum_{j=1}^n [K_{G,t}(\theta, \theta_t^j) G(\theta_t^j)^{-1} \nabla \log p(\theta_t^j) + \nabla_{\theta_t^j} \cdot (K_{G,t}(\theta, \theta_t^j) G(\theta_t^j)^{-1})]$ (see (15))
return $\{x_{T+1}^i\}_{i=1}^n$.

A Mirror Descent, Riemannian Gradient Flow, and Natural Gradient

The equivalence between the mirror flow $d\eta_t = -\nabla f(\theta_t)dt$, $\theta_t = \nabla\psi^*(\eta_t)dt$ and the Riemannian gradient flow in (3) is a direct result of the chain rule:

$$\frac{d\theta_t}{dt} = -\nabla_{\eta_t} \theta_t \frac{d\eta_t}{dt} = -(\nabla_{\theta_t} \eta_t)^{-1} \frac{d\eta_t}{dt} = -\nabla^2 \psi(\theta_t)^{-1} \nabla f(\theta_t), \quad (17)$$

$$\frac{d\eta_t}{dt} = -\nabla f(\theta_t) = -\nabla_{\theta_t} \eta_t \nabla_{\eta_t} f(\nabla\psi^*(\eta_t)) = -\nabla^2 \psi^*(\eta_t)^{-1} \nabla_{\eta_t} f(\nabla\psi^*(\eta_t)). \quad (18)$$

Depending on discretizing (17) or (18), there are two natural gradient descent (NGD) updates that can arise from the same gradient flow:

$$\text{NGD (a): } \theta_{t+1} = \theta_t - \epsilon_t \nabla^2 \psi(\theta_t)^{-1} \nabla f(\theta_t),$$

$$\text{NGD (b): } \eta_{t+1} = \eta_t - \epsilon_t \nabla^2 \psi^*(\eta_t)^{-1} \nabla_{\eta_t} f(\nabla\psi^*(\eta_t)).$$

With finite step sizes ϵ_t , their updates need not be the same and can lead to different optimization paths. Since $\nabla f(\theta_t) = \nabla^2 \psi^*(\eta_t)^{-1} \nabla_{\eta_t} f(\nabla\psi^*(\eta_t))$, NGD (b) is equivalent to the dual-space update by mirror descent. This relationship was pointed out in [54] and has been used for developing natural gradient variational inference algorithms [38]. We emphasize, however, our SVNG algorithm developed in Sec. 4.4 corresponds to the discretization in the primal space as in NGD (a). Therefore, it does not require an explicit dual space, and allows replacing $\nabla^2 \psi$ with more general information metric tensors.

B Riemannian Langevin Diffusions and Mirror-Langevin Diffusions

Zhang et al. [70] pointed out (4) is a particular case of the Riemannian LD. However, they did not give an explicit derivation. The Riemannian LD [53, 69, 46] with $\nabla^2 \psi(\cdot)$ as metric tensor is

$$d\theta_t = (\nabla^2 \psi(\theta_t)^{-1} \nabla \log p(\theta_t) + \nabla \cdot \nabla^2 \psi(\theta_t)^{-1})dt + \sqrt{2} \nabla^2 \psi(\theta_t)^{-1/2} dB_t. \quad (19)$$

To see the connection with mirror-Langevin diffusion, we would like to obtain the SDE that describes the evolution of $\eta_t = \nabla\psi(\theta_t)$ under the diffusion. This requires the following theorem that provides the analog of the ‘‘chain rule’’ in SDEs.

Theorem 9 (Itô formula [52, Thm 4.2.1]). *Let $(x_t)_{t \geq 0}$ be an Itô process in $\mathcal{X} \subset \mathbb{R}^d$ satisfying $dx_t = b(x_t)dt + \sigma(x_t)dB_t$. Let $f(x) \in C^2 : \mathbb{R}^d \rightarrow \mathbb{R}^d$. Then $y_t = f(x_t)$ is again an Itô process, and its i -th dimension satisfies*

$$dy_{t,i} = (\nabla f_i(x_t))^\top b(x_t) + \frac{1}{2} \text{Tr}(\nabla^2 f_i(x_t) \sigma(x_t) \sigma(x_t)^\top) dt + \nabla f_i(x_t)^\top \sigma(x_t) dB_t.$$

Substituting $\nabla\psi$ for f in Thm. 9, we have the SDE of $\eta_t = \nabla\psi(\theta_t)$ as

$$d\eta_t = (\nabla \log p(\theta_t) + \nabla^2 \psi(\theta_t) \nabla \cdot \nabla^2 \psi(\theta_t)^{-1} + h(\theta_t))dt + \nabla^2 \psi(\theta_t)^{1/2} dB_t,$$

where $h(\theta_t)_i = \text{Tr}(\nabla_{\theta_t}^2 (\nabla_{\theta_t, i} \psi(\theta_t)) \nabla^2 \psi(\theta_t)^{-1})$. Moreover, we have

$$\begin{aligned} & [\nabla^2 \psi(\theta_t) \nabla \cdot \nabla^2 \psi(\theta_t)^{-1}]_i + \text{Tr}(\nabla_{\theta_t}^2 (\nabla_{\theta_t, i} \psi(\theta_t)) \nabla^2 \psi(\theta_t)^{-1}) \\ &= \sum_{\ell=1}^d \sum_{j=1}^d \nabla^2 \psi(\theta_t)_{ij} \nabla_{\theta_t, \ell} [\nabla^2 \psi(\theta_t)^{-1}]_{j\ell} + \sum_{\ell=1}^d \sum_{j=1}^d \nabla_{\theta_t, \ell} \nabla^2 \psi(\theta_t)_{ij} [\nabla^2 \psi(\theta_t)^{-1}]_{j\ell} \\ &= \sum_{\ell=1}^d \nabla_{\theta_t, \ell} \left(\sum_{j=1}^d \nabla^2 \psi(\theta_t)_{ij} [\nabla^2 \psi(\theta_t)^{-1}]_{j\ell} \right) = \sum_{\ell=1}^d \nabla_{\theta_t, \ell} I_{i\ell} = 0. \end{aligned}$$

Therefore, the η_t diffusion is described by the SDE:

$$d\eta_t = \nabla \log p(\theta_t) dt + \nabla^2 \psi(\theta_t)^{1/2} dB_t, \quad \theta_t = \nabla \psi^*(\eta_t).$$

C Derivation of the Mirrored Stein Operator

The following theorem characterizes the generator of processes described by the SDEs.

Theorem 10 (Generator of Itô diffusion [52, Thm 7.3.3]). *Let $(x_t)_{t \geq 0}$ be the Itô diffusion in $\mathcal{X} \subseteq \mathbb{R}^d$ satisfying $dx_t = b(x_t)dt + \sigma(x_t)dB_t$. For any $f \in C_c^2(\mathcal{X})$, the (infinitesimal) generator A of $(x_t)_{t \geq 0}$ is*

$$(Af)(x) = b(x)^\top \nabla f(x) + \frac{1}{2} \text{Tr}(\sigma(x)\sigma(x)^\top \nabla^2 f(x)).$$

According to Thm. 10, the generator of the mirror-Langevin diffusion described by (19) is

$$\begin{aligned} (A_{p,\psi}f)(\theta) &= (\nabla^2 \psi(\theta)^{-1} \nabla \log p(\theta) + \nabla \cdot \nabla^2 \psi(\theta)^{-1})^\top \nabla f(\theta) + \text{Tr}(\nabla^2 \psi(\theta)^{-1} \nabla^2 f(\theta)) \\ &= \nabla f(\theta)^\top \nabla^2 \psi(\theta)^{-1} \nabla \log p(\theta) + \nabla \cdot (\nabla^2 \psi(\theta)^{-1} \nabla f(\theta)). \end{aligned}$$

Now substituting $g(\theta)$ for $\nabla f(\theta)$, we obtain the associated mirrored Stein operator:

$$(\mathcal{M}_{p,\psi}g)(\theta) = g(\theta)^\top \nabla^2 \psi(\theta)^{-1} \nabla \log p(\theta) + \nabla \cdot (\nabla^2 \psi(\theta)^{-1} g(\theta)).$$

D Background on Reproducing Kernel Hilbert Spaces

Let \mathcal{H} be a Hilbert space of functions defined on \mathcal{X} and taking their values in \mathbb{R} . We say k is a reproducing kernel (or kernel) of \mathcal{H} if $\forall x \in \mathcal{X}, k(x, \cdot) \in \mathcal{H}$ and $\forall f \in \mathcal{H}, \langle f, k(x, \cdot) \rangle_{\mathcal{H}} = f(x)$. \mathcal{H} is called a reproducing kernel Hilbert space (RKHS) if it has a kernel. Kernels are positive definite (p.d.) functions, which means that matrices with the form $(k(x_i, x_j))_{ij}$ are positive semidefinite. For any p.d. function k , there is a unique RKHS with k as the reproducing kernel, which can be constructed by the completion of $\{\sum_{i=1}^n a_i k(x_i, \cdot), x_i \in \mathcal{X}, a_i \in \mathbb{R}, i \in \mathbb{N}\}$.

Now we assume \mathcal{X} is a metric space, k is a bounded continuous kernel with the RKHS \mathcal{H} , and ν is a positive measure on \mathcal{X} . $L^2(\nu)$ denote the space of all square-integrable functions w.r.t. ν . Then the kernel integral operator $T_k : L^2(\nu) \rightarrow L^2(\nu)$ defined by

$$T_k g = \int_{\mathcal{X}} g(x) k(x, \cdot) d\nu$$

is compact and self-adjoint. Therefore, according to the spectral theorem, there exists an at most countable set of positive eigenvalues $\{\lambda_j\}_{j \in J} \subset \mathbb{R}$ with $\lambda_1 \geq \lambda_2 \geq \dots$ converging to zero and orthonormal eigenfunctions $\{u_j\}_{j \in J}$ such that

$$T_k u_j = \lambda_j u_j,$$

and k has the representation $k(x, x') = \sum_{j \in J} \lambda_j u_j(x) u_j(x')$ (Mercer's theorem on non-compact domains), where the convergence of the sum is absolute and uniform on compact subsets of $\mathcal{X} \times \mathcal{X}$ [22].

E Supplementary Experimental Details and Additional Results

In this section, we report supplementary details and additional results from the experiments of Sec. 5. In Secs. 5.1 and 5.2, we use the inverse multiquadric input kernel $k(\theta, \theta') = (1 + \|\theta - \theta'\|_2^2 / \ell^2)^{-1/2}$ due to its convergence control properties [27]. In the unconstrained experiments of Sec. 5.3, we use the Gaussian kernel $k(\theta, \theta') = \exp(-\|\theta - \theta'\|_2^2 / \ell^2)$ for consistency with past work. The bandwidth ℓ is determined by the median heuristic [25]. We select τ from $\{0.98, 0.99\}$ for all SVM experiments. For unconstrained targets, we report, for each method, results from the best fixed step size $\epsilon \in \{0.01, 0.05, 0.1, 0.5, 1\}$ selected on a separate validation set. For constrained targets, we select step sizes adaptively to accommodate rapid density growth near the boundary; specifically, we use RMSProp [31], an extension of the AdaGrad algorithm [17] used in [44], and report performance with the best learning rate. Results were recorded on an Intel(R) Xeon(R) CPU E5-2690 v4 @ 2.60GHz and an NVIDIA Tesla P100 PCIe 16GB.

E.1 Approximation quality on the simplex

The sparse Dirichlet posterior of [53] extended to 20 dimensions features a sparse, symmetric $\text{Dir}(\alpha)$ prior with $\alpha_k = 0.1$ for $k \in \{1, \dots, 20\}$ and sparse count data $n_1 = 90$, $n_2 = n_3 = 5$, $n_j = 0$ ($j > 3$), modeled via a multinomial likelihood. The quadratic target satisfies $\log p(\theta) = -\frac{1}{2\sigma^2}\theta^\top A\theta + \text{const}$, where we slightly modify the target density of [1] to make it less flat by introducing a scale parameter $\sigma = 0.01$. $A \in \mathbb{R}^{19 \times 19}$ is a positive definite matrix generated by normalizing products of random matrices with i.i.d. elements drawn from $\text{Unif}[-1, 1]$.

We initialize all methods with i.i.d. samples from $\text{Dirichlet}(5)$ to prevent any of the initial particles being too close to the boundary. For each method and each learning rate we apply 500 particle updates. For SVMd we set $\tau = 0.98$. We search the base learning rates of RMSProp in $\{0.1, 0.01, 0.001\}$ for SVMd and MSVGD. Since projected SVGD applies updates in the θ space, the appropriate learning rate range is smaller than those of SVMd and MSVGD. There we search the base learning rate of RMSProp in $\{0.01, 0.001, 0.0001\}$. For all methods the results under each base learning rate are plotted in Fig. 6.

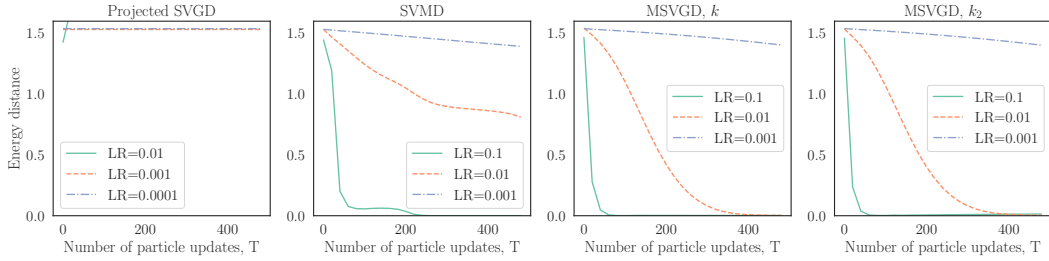


Figure 6: Sampling from a Dirichlet target on a 20-simplex. We plot the energy distance to a ground truth sample of size 1000.

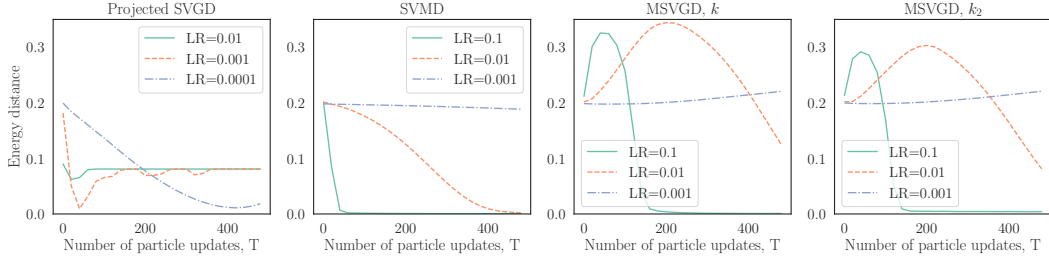


Figure 7: Sampling from a quadratic target on a 20-simplex. We plot the energy distance to a ground truth sample of size 1000 drawn by NUTS [32].

E.2 Confidence intervals for post-selection inference

Given a dataset $X \in \mathbb{R}^{\tilde{n} \times p}$, $y \in \mathbb{R}^{\tilde{n}}$, the randomized Lasso [63] solves the following problem:

$$\operatorname{argmin}_{\beta \in \mathbb{R}^p} \frac{1}{2} \|y - X\beta\|_2^2 + \lambda \|\beta\|_1 - w^\top \beta + \frac{\epsilon}{2} \|\beta\|_2^2, \quad w \sim \mathbb{G}.$$

where \mathbb{G} is a user-specified log-concave distribution with density g . We choose \mathbb{G} to be zero-mean independent Gaussian distributions while leaving its scale and the ridge parameter ϵ to be automatically determined by the `randomizedLasso` function of the `selectiveInference` package. We initialize the particles of our SVMd and MSVGD in the following way: First, we map the solution $\hat{\beta}_E$ to the dual space by $\nabla\psi$. Next, we add i.i.d. standard Gaussian noise to n copies of the image in the dual space. Finally, we map the n particles back to the primal space by $\nabla\psi^*$ and use them as the initial locations. Below we discuss the remaining settings and additional results of the simulation and the HIV-1 drug resistance experiment separately.

Simulation In our simulation we mostly follow the settings of [57] except using a different penalty level λ recommended in the `selectiveInference` R package. We set $\tilde{n} = 100$ and $p = 40$. The

design matrix X is generated from an equi-correlated model, i.e., each datapoint $x_i \in \mathbb{R}^p$ is generated i.i.d. from $\mathcal{N}(0, \Sigma)$ with $\Sigma_{ii} = 1, \Sigma_{ij} = 0.3$ ($i \neq j$) and then normalized to have almost unit length. The normalization is done by first centering each dimension by subtracting the mean and dividing the standard deviation of that column of X , then additionally multiplying $1/\tilde{n}^{1/2}$. y is generated from a standard Gaussian which is independent of X , i.e., we assume the global null setting where the true value of β is zero. We set λ to be the value returned by `theoretical.lambda` of the `selectiveInference` R package multiplied a coefficient $0.7\tilde{n}$, where the 0.7 adjustment is introduced in the test examples of the R package to reduce the regularization effect so that we have a reasonably large set of selected features when $p = 40$. The base learning rates for SVM and MSVGD are set to 0.01 and we run them for $T = 1000$ particle updates. τ is set to 0.98 for SVM.

Our 2D example in Fig. 4a is grabbed from one run of the simulation where there happen to be only 2 features selected by the randomized Lasso. The selective distribution in this case has log-density $\log p(\theta) = -8.07193((2.39859\theta_1 + 1.90816\theta_2 + 2.39751)^2 + (1.18099\theta_2 - 1.46104)^2) + \text{const}, \theta_{1,2} \geq 0$.

The error bars for actual coverage levels in Fig. 3a and Fig. 3b are 95% Wilson intervals [68], which is known to be more accurate than ± 2 standard deviation intervals for binomial proportions like the coverage. In Fig. 8a and Fig. 8b we additionally plot the average length of the confidence intervals w.r.t. different sample size N and nominal coverage levels. For all three methods the CI widths are very close, although MSVGD consistently has wider intervals than SVM and `selectiveInference`. This indicates that SVM can be preferred over MSVGD when both methods produce coverage above the nominal level.

HIV-1 drug resistance We take the vitro measurement of log-fold change under the 3TC drug as response and include mutations that had appeared 11 times in the dataset as regressors. This results in $\tilde{n} = 663$ datapoints with $p = 91$ features. We choose λ to be the value returned by `theoretical.lambda` of the `selectiveInference` R package multiplied by \tilde{n} . The base learning rates for SVM and MSVGD are set to 0.01 and we run them for $T = 2000$ particle updates. τ is set to 0.99 for SVM.

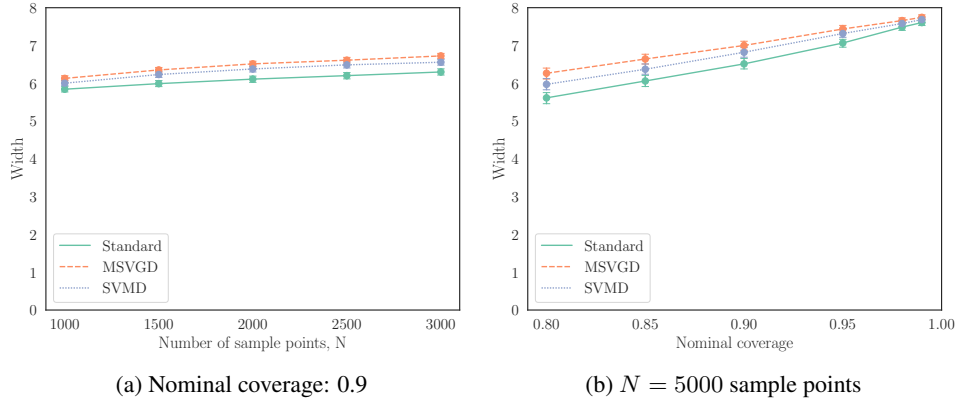


Figure 8: Width of post-selection CIs across (a) 500 / (b) 200 replications of simulation of [57].

E.3 Large-scale posterior inference with non-Euclidean geometry

The Bayesian logistic regression model we consider is $\prod_{i=1}^{\tilde{n}} p(y_i|x_i, w)p(w)$, where $p(w) = \mathcal{N}(w|0, I)$, $p(y_i|x_i, w) = \text{Bernoulli}(\sigma(w^\top x_i))$. The bias parameter is absorbed into w by adding an additional feature 1 to each x_i . The gradient of the log density of the posterior distribution of w is $\nabla_w \log p(w|\{y_i, x_i\}_{i=1}^N) = \sum_{i=1}^N x_i(y_i - \sigma(w^\top x_i)) - w$. We choose the metric tensor

$\nabla^2\psi(w)$ to be the Fisher information matrix (FIM) of the likelihood:

$$\begin{aligned} F &= \frac{1}{\tilde{n}} \sum_{i=1}^{\tilde{n}} \mathbb{E}_{p(y_i|w, x_i)} [\nabla_w \log p(y_i|x_i, w) \nabla_w \log p(y_i|x_i, w)^\top] \\ &= \frac{1}{\tilde{n}} \sum_{i=1}^{\tilde{n}} \sigma(w^\top x_i) (1 - \sigma(w^\top x_i)) x_i x_i^\top. \end{aligned}$$

Following [66], for each iteration r ($r \geq 1$), we estimate the sum with a stochastic minibatch \mathcal{B}_r of size 256: $\hat{F}_{\mathcal{B}_r} = \frac{\tilde{n}}{|\mathcal{B}_r|} \sum_{i \in \mathcal{B}_r} \sigma(w^\top x_i) (1 - \sigma(w^\top x_i)) x_i x_i^\top$ and approximate the FIM with a moving average across iterations:

$$\hat{F}_r = \rho_r \hat{F}_{r-1} + (1 - \rho_r) \hat{F}_{\mathcal{B}_r}, \quad \text{where } \rho_r = \min(1 - 1/r, 0.95).$$

To ensure the positive definiteness of the FIM, a damping term $0.01I$ is added before taking the inverse. For RSVG and SVNG, the gradient of the inverse of FIM is estimated with $\nabla_{w_j} F^{-1} \approx -\hat{F}_r^{-1} (\hat{\nabla}_{w_j}^r F) \hat{F}_r^{-1}$, where $\hat{\nabla}_{w_j}^r F = \rho_r \hat{\nabla}_{w_j}^{r-1} F + (1 - \rho_r) \nabla_{w_j} \hat{F}_{\mathcal{B}_r}$.

We run each method for $T = 3000$ particle updates with learning rates in $\{0.01, 0.05, 0.1, 0.5, 1\}$ and average the results for 5 random trials. τ is set to 0.98 for SVNG. For each run, we randomly keep 20% of the dataset as test data, 20% of the remaining points as the validation set, and all the rest as the training set. The results of each method on validation sets with all choices of learning rates are plotted in Fig. 9. We see that the SVNG updates are very robust to the change in learning rates and is able to accommodate very large learning rates (up to 1) without a significant loss in performance. The results in Fig. 5 are reported with the learning rate that performs best on the validation set.

F Proofs

F.1 Proof of Prop. 1

Proof Fix any $g \in \mathcal{G}_\psi$. Since g and ∇g are bounded and $\nabla^2\psi(\theta)^{-1} \nabla \log p(\theta)$ and $\nabla \cdot \nabla^2\psi(\theta)^{-1}$ are p -integrable, the expectation $\mathbb{E}_p[(\mathcal{M}_{p, \psi, g})(\theta)]$ exists. Because Θ is convex, Θ_r is bounded and convex with Lipschitz boundary. Since $p \nabla^2\psi^{-1} g \in C^1$, we have

$$\begin{aligned} |\mathbb{E}_p[(\mathcal{M}_{p, \psi, g})(\theta)]| &= |\mathbb{E}_p[g(\theta)^\top \nabla^2\psi(\theta)^{-1} \nabla \log p(\theta) + \nabla \cdot (\nabla^2\psi(\theta)^{-1} g(\theta))]| \\ &= \left| \int_{\Theta} \nabla p(\theta)^\top \nabla^2\psi(\theta)^{-1} g(\theta) + p(\theta) \nabla \cdot (\nabla^2\psi(\theta)^{-1} g(\theta)) d\theta \right| \\ &= \left| \int_{\Theta} \nabla \cdot (p(\theta) \nabla^2\psi(\theta)^{-1} g(\theta)) d\theta \right| \\ &= \left| \lim_{r \rightarrow \infty} \int_{\Theta_r} \nabla \cdot (p(\theta) \nabla^2\psi(\theta)^{-1} g(\theta)) d\theta \right| \quad (\text{by dominated convergence}) \\ &= \left| \lim_{r \rightarrow \infty} \int_{\partial\Theta_r} (p(\theta) \nabla^2\psi(\theta)^{-1} g(\theta))^\top n_r(\theta) d\theta \right| \quad (\text{by the divergence theorem}) \\ &\leq \lim_{r \rightarrow \infty} \int_{\partial\Theta_r} p(\theta) \|g(\theta)\|_2 \|\nabla^2\psi(\theta)^{-1} n_r(\theta)\|_2 d\theta \quad (\text{by Cauchy-Schwarz}) \\ &\leq \|g\|_\infty \lim_{r \rightarrow \infty} \int_{\partial\Theta_r} p(\theta) \|\nabla^2\psi(\theta)^{-1} n_r(\theta)\|_2 d\theta = 0 \quad (\text{by assumption}). \end{aligned}$$

□

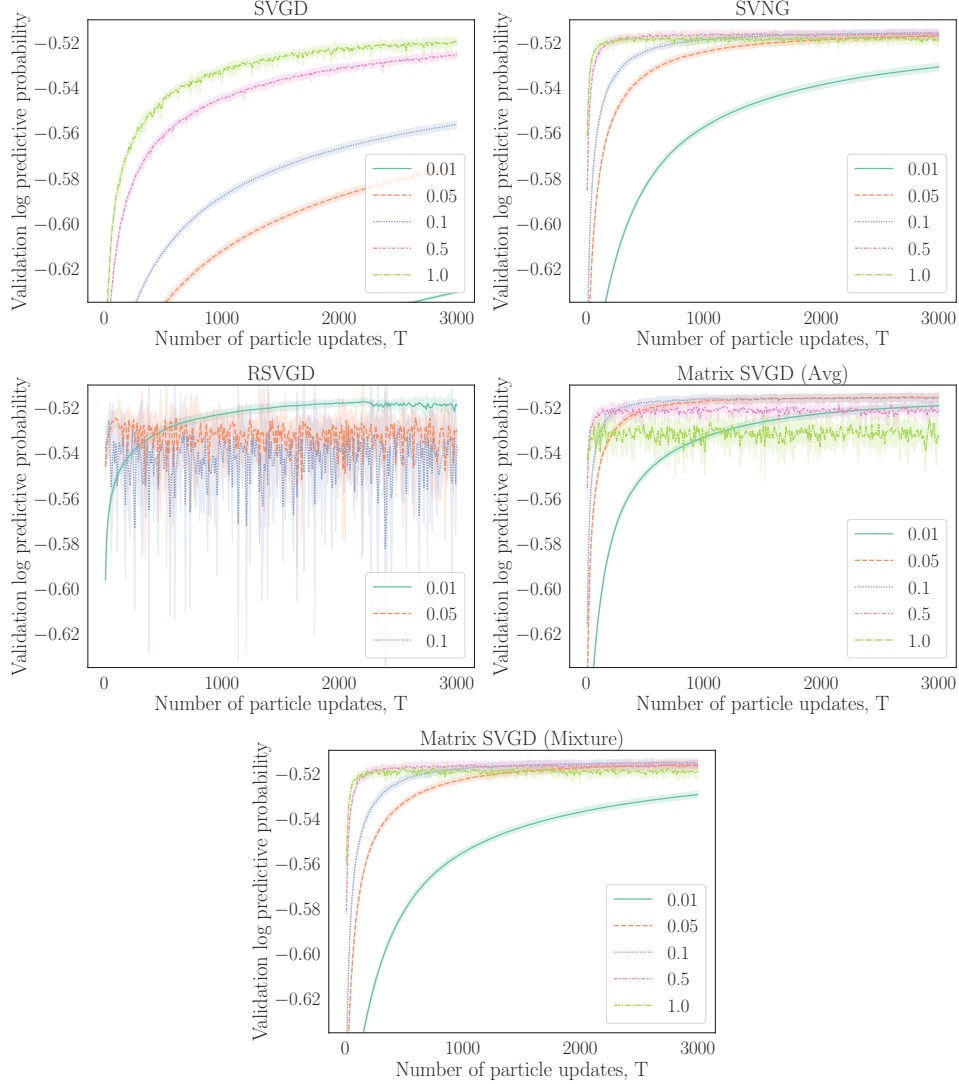


Figure 9: Logistic regression results on validation sets with learning rates in $\{0.01, 0.05, 0.1, 0.5, 1\}$. Running RSVG with learning rates 0.5 and 1 produces numerical errors. Therefore, we did not include them in the plot.

F.2 Proof of Thm. 3: Optimal mirror updates in RKHS

Proof Let e_i denote the standard basis vector of \mathbb{R}^d with the i -th element being 1 and others being zeros. Since $m \in \mathcal{H}_K$, we have

$$\begin{aligned}
m(\theta)^\top \nabla^2 \psi(\theta)^{-1} \nabla \log p(\theta) &= \langle m, K(\cdot, \theta) \nabla^2 \psi(\theta)^{-1} \nabla \log p(\theta) \rangle_{\mathcal{H}_K} \\
\nabla \cdot (\nabla^2 \psi(\theta)^{-1} m(\theta)) &= \sum_{i=1}^d \nabla_{\theta_i} (m(\theta)^\top \nabla^2 \psi(\theta)^{-1} e_i) \\
&= \sum_{i=1}^d \langle m, \nabla_{\theta_i} (K(\cdot, \theta) \nabla^2 \psi(\theta)^{-1} e_i) \rangle_{\mathcal{H}_K} \\
&= \langle m, \nabla_{\theta} \cdot (K(\cdot, \theta) \nabla^2 \psi(\theta)^{-1}) \rangle_{\mathcal{H}_K},
\end{aligned}$$

where we define the divergence of a matrix as a vector whose elements are the divergences of each row of the matrix. Then, we write (10) as

$$\begin{aligned}
& -\mathbb{E}_{q_t}[m(\theta)^\top \nabla^2 \psi(\theta)^{-1} \nabla \log p(\theta) + \nabla \cdot (\nabla^2 \psi(\theta)^{-1} m(\theta))] \\
& = -\mathbb{E}_{q_t}[\langle m, K(\cdot, \theta) \nabla^2 \psi(\theta)^{-1} \nabla \log p(\theta) + \nabla_\theta \cdot (K(\cdot, \theta) \nabla^2 \psi(\theta)^{-1}) \rangle_{\mathcal{H}_K}] \\
& = -\langle m, \mathbb{E}_{q_t}[K(\cdot, \theta) \nabla^2 \psi(\theta)^{-1} \nabla \log p(\theta) + \nabla_\theta \cdot (K(\cdot, \theta) \nabla^2 \psi(\theta)^{-1})] \rangle_{\mathcal{H}_K} \\
& = -\langle m, \mathbb{E}_{q_t}[\mathcal{M}_{p, \psi} K(\cdot, \theta)] \rangle_{\mathcal{H}_K}.
\end{aligned}$$

Therefore, the optimal direction in the \mathcal{H}_K norm ball $\mathcal{B}_{\mathcal{H}_K} = \{g : \|g\|_{\mathcal{H}_K} \leq 1\}$ that minimizes (10) is $g_t^* \propto g_{q_t, K}^* = \mathbb{E}_{q_t}[\mathcal{M}_{p, \psi} K(\cdot, \theta)]$. \square

E.3 Proof of Thm. 4: Mirrored SVGD updates

Proof A p.d. kernel k composed with any map ϕ is still a p.d. kernel. To prove this, let $\{x_1, \dots, x_p\} = \{\phi(\eta_1), \dots, \phi(\eta_m)\}$, $p \leq m$. Then

$$\sum_{i, j} \alpha_i \alpha_j k(\phi(\eta_i), \phi(\eta_j)) = \sum_{\ell, m} \beta_\ell \beta_m k(x_\ell, x_m) \geq 0,$$

where $\beta_\ell = \sum_{i \in S_\ell} \alpha_i$, $S_\ell = \{i : \phi(\eta_i) = x_\ell\}$. Therefore, $k_\psi(\eta, \eta') = k(\nabla \psi^*(\eta), \nabla \psi^*(\eta'))$ is a p.d. kernel. Plugging $K = kI$ into Lem. 11, we have

$$\begin{aligned}
g_{q_t, K_k}^*(\theta_t) & = \mathbb{E}_{q_{t, H}}[K_{\nabla \psi^*}(\nabla \psi(\theta_t), \eta) \nabla \log p_H(\eta) + \nabla_\eta \cdot K_{\nabla \psi^*}(\nabla \psi(\theta_t), \eta)] \\
& = \mathbb{E}_{q_{t, H}}[k(\nabla \psi^*(\eta_t), \nabla \psi^*(\eta)) \nabla \log p_H(\eta) + \sum_{j=1}^d \nabla_{\eta_j} k(\nabla \psi^*(\eta_t), \nabla \psi^*(\eta)) e_j] \\
& = \mathbb{E}_{q_{t, H}}[k_\psi(\eta_t, \eta) \nabla \log p_H(\eta) + \nabla_\eta k_\psi(\eta_t, \eta)].
\end{aligned}$$

\square

E.4 Proof of Thm. 6: Convergence of mirrored updates as $n \rightarrow \infty$

Proof The idea is to reinterpret our mirrored updates as one step of a matrix SVGD in η space based on Lem. 11 and then follow the path of [29, Thm. 7]. Assume that $q_{t, H}^n$ and $q_{t, H}^\infty$ have integrable means. Let η^n, η^∞ be an optimal Wasserstein-1 coupling of $q_{t, H}^n$ and $q_{t, H}^\infty$. Let Φ_{q_t, K_t} denote the transform through one step of mirrored update: $\theta_t = \nabla \psi^*(\eta_t)$, $\eta_{t+1} = \eta_t + \epsilon_t g_{q_t, K_t}^*(\theta_t)$. Then, with Lem. 11, we have

$$\begin{aligned}
& \|\Phi_{q_t, K_t}(\eta) - \Phi_{q_t, K_t}(\eta')\|_2 \\
& = \|\eta + \epsilon_t g_{q_t, K_t}^*(\theta) - \eta' - \epsilon_t g_{q_t, K_t}^*(\theta')\|_2 \\
& \leq \|\eta - \eta'\|_2 + \epsilon_t \|g_{q_t, K_t}^*(\theta) - g_{q_t, K_t}^*(\theta')\|_2 \\
& \leq \|\eta - \eta'\|_2 \\
& + \epsilon_t \|\mathbb{E}_{\eta^n}[K_{\nabla \psi^*, t}(\eta, \eta^n) \nabla \log p_H(\eta^n) + \nabla_{\eta^n} \cdot K_{\nabla \psi^*, t}(\eta, \eta^n) \\
& \quad - (K_{\nabla \psi^*, t}(\eta', \eta^n) \nabla \log p_H(\eta^n) + \nabla_{\eta^n} \cdot K_{\nabla \psi^*, t}(\eta', \eta^n))]\|_2 \\
& + \epsilon_t \|\mathbb{E}_{\eta^n, \eta^\infty}[K_{\nabla \psi^*, t}(\eta', \eta^n) \nabla \log p_H(\eta^n) + \nabla_{\eta^n} \cdot K_{\nabla \psi^*, t}(\eta', \eta^n) \\
& \quad - (K_{\nabla \psi^*, t}(\eta', \eta^\infty) \nabla \log p_H(\eta^\infty) + \nabla_{\eta^\infty} \cdot K_{\nabla \psi^*, t}(\eta', \eta^\infty))]\|_2 \\
& \leq \|\eta - \eta'\|_2 + \epsilon_t c_1 (1 + \mathbb{E}[\|\eta^n\|_2]) \|\eta - \eta'\|_2 + \epsilon_t c_2 (1 + \|\eta'\|_2) \mathbb{E}_{\eta^n, \eta^\infty}[\|\eta^n - \eta^\infty\|_2] \\
& = \|\eta - \eta'\|_2 + \epsilon_t c_1 (1 + \mathbb{E}_{q_{t, H}^n}[\|\cdot\|_2]) \|\eta - \eta'\|_2 + \epsilon_t c_2 (1 + \|\eta'\|_2) W_1(q_{t, H}^n, q_{t, H}^\infty).
\end{aligned}$$

Since $\Phi_{q_t, K_t}(\eta^n) \sim q_{t+1, H}^n$, $\Phi_{q_t, K_t}(\eta^\infty) \sim q_{t+1, H}^\infty$, we conclude

$$\begin{aligned}
& W_1(q_{t+1, H}^n, q_{t+1, H}^\infty) \\
& \leq \mathbb{E}[\|\Phi_{q_t, K_t}(\eta^n) - \Phi_{q_t, K_t}(\eta^\infty)\|_2] \\
& \leq (1 + \epsilon_t c_1 (1 + \mathbb{E}_{q_{t, H}^n}[\|\cdot\|_2])) \mathbb{E}[\|\eta^n - \eta^\infty\|_2] + \epsilon_t c_2 (1 + \|\eta'\|_2) W_1(q_{t, H}^n, q_{t, H}^\infty) \\
& \leq (1 + \epsilon_t c_1 (1 + \mathbb{E}_{q_{t, H}^n}[\|\cdot\|_2]) + \epsilon_t c_2 (1 + \mathbb{E}_{q_{t, H}^\infty}[\|\cdot\|_2])) W_1(q_{t, H}^n, q_{t, H}^\infty).
\end{aligned}$$

The final claim $q_t^n \Rightarrow q_t^\infty$ now follows by the continuous mapping theorem as $\nabla\psi^*$ is continuous. \square

F.5 Proof of Thm. 7: Infinite-particle mirrored Stein updates decrease KL and MKSD

Proof Let $T_{q_t^\infty, K_t}$ denote transform of the density function through one step of mirrored update: $\theta_t = \nabla\psi^*(\eta_t)$, $\eta_{t+1} = \eta_t + \epsilon_t g_{q_t^\infty, K_t}^*(\theta_t)$. Then

$$\begin{aligned} & \text{KL}(q_{t+1}^\infty \| p) - \text{KL}(q_t^\infty \| p) \\ &= \text{KL}(q_t^\infty \| T_{q_t^\infty, K_t}^{-1} p) - \text{KL}(q_t^\infty \| p) \\ &= \mathbb{E}_{\eta_t \sim q_{t,H}^\infty} [\log p_H(\eta_t) - \log p_H(\eta_t + \epsilon_t g_{q_t^\infty, K_t}^*(\theta_t)) - \log |\det(I + \epsilon_t \nabla_{\eta_t} g_{q_t^\infty, K_t}^*(\theta_t))|], \end{aligned}$$

where we have used the invariance of KL divergence under reparameterization: $\text{KL}(q_t \| p) = \text{KL}(q_{t,H} \| p_H)$. Following [43], we bound the difference of the first two terms as

$$\begin{aligned} & \log p_H(\eta_t) - \log p_H(\eta_t + \epsilon_t g_{q_t^\infty, K_t}^*(\theta_t)) \\ &= - \int_0^1 \nabla_s \log p_H(\eta_t(s)) ds, \quad \text{where } \eta_t(s) \triangleq \eta_t + s \epsilon_t g_{q_t^\infty, K_t}^*(\theta_t) \\ &= - \int_0^1 \nabla \log p_H(\eta_t(s))^\top (\epsilon_t g_{q_t^\infty, K_t}^*(\theta_t)) ds \\ &= -\epsilon_t \nabla \log p_H(\eta_t)^\top g_{q_t^\infty, K_t}^*(\theta_t) + \int_0^1 (\nabla \log p_H(\eta_t) - \nabla \log p_H(\eta_t(s)))^\top (\epsilon_t g_{q_t^\infty, K_t}^*(\theta_t)) ds \\ &\leq -\epsilon_t \nabla \log p_H(\eta_t)^\top g_{q_t^\infty, K_t}^*(\theta_t) + \epsilon_t \int_0^1 \|\nabla \log p_H(\eta_t) - \nabla \log p_H(\eta_t(s))\|_2 \cdot \|g_{q_t^\infty, K_t}^*(\theta_t)\|_2 ds \\ &\leq -\epsilon_t \nabla \log p_H(\eta_t)^\top g_{q_t^\infty, K_t}^*(\theta_t) + \frac{L\epsilon_t^2}{2} \|g_{q_t^\infty, K_t}^*(\theta_t)\|_2^2, \end{aligned}$$

and bound the log determinant term using Lem. 13:

$$-\log |\det(I + \epsilon_t \nabla_{\eta_t} g_{q_t^\infty, K_t}^*(\theta_t))| \leq -\epsilon_t \text{Tr}(\nabla_{\eta_t} g_{q_t^\infty, K_t}^*(\theta_t)) + 2\epsilon_t^2 \|\nabla_{\eta_t} g_{q_t^\infty, K_t}^*(\theta_t)\|_F^2.$$

The next thing to notice is that $\mathbb{E}_{\eta_t \sim q_{t,H}^\infty} [\nabla \log p_H(\eta_t)^\top g_{q_t^\infty, K_t}^*(\theta_t) + \text{Tr}(\nabla_{\eta_t} g_{q_t^\infty, K_t}^*(\theta_t))]$ is the square of the MKSD in (16). We can show this equivalence using the identity proved in Lem. 12:

$$\begin{aligned} & \mathbb{E}_{\eta_t \sim q_{t,H}^\infty} [g_{q_t^\infty, K_t}^*(\theta_t)^\top \nabla \log p_H(\eta_t) + \text{Tr}(\nabla_{\eta_t} g_{q_t^\infty, K_t}^*(\theta_t))] \\ &= \mathbb{E}_{\theta_t \sim q_t^\infty} [g_{q_t^\infty, K_t}^*(\theta_t)^\top \nabla^2 \psi(\theta_t)^{-1} \nabla_{\theta_t} (\log p(\theta_t) - \log \det \nabla^2 \psi(\theta_t)) \\ &\quad + \text{Tr}(\nabla^2 \psi(\theta_t)^{-1} \nabla g_{q_t^\infty, K_t}^*(\theta_t))] \\ &= \mathbb{E}_{\theta_t \sim q_t^\infty} [g_{q_t^\infty, K_t}^*(\theta_t)^\top \nabla^2 \psi(\theta_t)^{-1} \nabla \log p(\theta_t) + \nabla \cdot (\nabla^2 \psi(\theta_t)^{-1} g_{q_t^\infty, K_t}^*(\theta_t))] \quad (\text{Lem. 12}) \\ &= \mathbb{E}_{\theta_t \sim q_t^\infty} [(\mathcal{M}_{p, \psi} g_{q_t^\infty, K_t}^*)(\theta_t)] \\ &= \text{MKSD}_{K_t}(q_t^\infty, p)^2. \end{aligned}$$

Finally, we are going to bound $\|g_{q_t^\infty, K_t}^*(\theta_t)\|_2^2$ and $\|\nabla_{\eta_t} g_{q_t^\infty, K_t}^*(\theta_t)\|_F^2$. From the assumptions we have ψ is α -strongly convex and thus ψ^* is $\frac{1}{\alpha}$ -strongly smooth [37], therefore $\|\nabla^2 \psi^*(\cdot)\|_2 \leq \frac{1}{\alpha}$. By Lem. 14, we know

$$\begin{aligned} \|g_{q_t^\infty, K_t}^*(\theta_t)\|_2^2 &\leq \|g_{q_t^\infty, K_t}^*\|_{\mathcal{H}_{K_t}}^2 \|K(\theta_t, \theta_t)\|_{\text{op}} = \text{MKSD}_{K_t}(q_t^\infty, p)^2 \|K_t(\theta_t, \theta_t)\|_{\text{op}}, \\ \|\nabla_{\eta_t} g_{q_t^\infty, K_t}^*(\theta_t)\|_F^2 &= \|\nabla^2 \psi^*(\eta_t) \nabla g_{q_t^\infty, K_t}^*(\theta_t)\|_F^2 \leq \|\nabla^2 \psi^*(\eta_t)\|_2^2 \|\nabla g_{q_t^\infty, K_t}^*(\theta_t)\|_F^2 \\ &\leq \frac{1}{\alpha^2} \|g_{q_t^\infty, K_t}^*\|_{\mathcal{H}_{K_t}}^2 \sum_{i=1}^d \|\nabla_{i, d+i}^2 K_t(\theta_t, \theta_t)\|_{\text{op}} \\ &= \frac{1}{\alpha^2} \text{MKSD}_{K_t}(q_t^\infty, p)^2 \sum_{i=1}^d \|\nabla_{i, d+i}^2 K_t(\theta_t, \theta_t)\|_{\text{op}}, \end{aligned}$$

where $\nabla_{i,d+i}^2 K(\theta, \theta)$ denotes $\nabla_{\theta_i, \theta'_i}^2 K(\theta, \theta')|_{\theta'=\theta}$. Combining all of the above, we have

$$\begin{aligned} & \text{KL}(q_{t+1}^\infty \| p) - \text{KL}(q_t^\infty \| p) \\ & \leq - \left(\epsilon_t - \frac{L\epsilon_t^2}{2} \sup_{\theta} \|K_t(\theta, \theta)\|_{\text{op}} - \frac{2\epsilon_t^2}{\alpha^2} \sum_{i=1}^d \sup_{\theta} \|\nabla_{i,d+i}^2 K_t(\theta, \theta)\|_{\text{op}} \right) \text{MKSD}_{K_t}(q_t^\infty, p)^2. \end{aligned}$$

Plugging in the definition of κ_1 and κ_2 finishes the proof. \square

F.6 Proof of Thm. 8: MKSD $_{K_k}$ determines weak convergence

Proof According to Thm. 4,

$$g_{q, K_k}^* = \mathbb{E}_{q_H} [k(\cdot, \nabla\psi^*(\eta)) \nabla \log p_H(\eta) + \nabla_{\eta} k(\nabla\psi^*(\eta), \cdot)],$$

where $q_H(\eta)$ denotes the density of $\eta = \nabla\psi(\theta)$ under the distribution $\theta \sim q$. From the assumptions we have $k(\theta, \theta') = \kappa(\nabla\psi(\theta), \nabla\psi(\theta'))$. With this specific choice of k , the squared MKSD is

$$\begin{aligned} \text{MKSD}_{K_k}(q, p)^2 &= \|g_{q, K_k}^*\|_{\mathcal{H}_{K_k}}^2 \\ &= \mathbb{E}_{\eta, \eta' \sim q_H} \left[\frac{1}{p_H(\eta)p_H(\eta')} \nabla_{\eta} \nabla_{\eta'} (p_H(\eta) k(\nabla\psi^*(\eta), \nabla\psi^*(\eta')) p_H(\eta')) \right] \\ &= \mathbb{E}_{\eta, \eta' \sim q_H} \left[\frac{1}{p_H(\eta)p_H(\eta')} \nabla_{\eta} \nabla_{\eta'} (p_H(\eta) \kappa(\eta, \eta') p_H(\eta')) \right]. \end{aligned} \quad (20)$$

The final expression in (20) is the squared kernel Stein discrepancy (KSD) [45, 13, 27] between q_H and p_H with the kernel κ : $\text{KSD}_{\kappa}(q_H, p_H)^2$. Recall that it is proved in [27, Theorem 8] that, for $\kappa(x, y) = (c^2 + \|x - y\|_2^2)^{\beta}$ with $\beta \in (-1, 0)$ and distantly dissipative p_H with Lipschitz score functions, $q_H \Rightarrow p_H$ if $\text{KSD}_{\kappa}(q_H, p_H) \rightarrow 0$. The advertised result ($q \Rightarrow p$ if $\text{MKSD}_{K_k}(q, p) \rightarrow 0$) now follows by the continuous mapping theorem as $\nabla\psi^*$ is continuous. \square

G Lemmas

Lemma 11. *Let $K_{\nabla\psi^*}(\eta, \eta') \triangleq K(\nabla\psi^*(\eta), \nabla\psi^*(\eta'))$. The mirrored updates $g_{q_t, K}^*$ in (11) can be equivalently expressed as*

$$g_{q_t, K}^* = \mathbb{E}_{q_t, H} [K_{\nabla\psi^*}(\nabla\psi(\cdot), \eta) \nabla \log p_H(\eta) + \nabla_{\eta} \cdot K_{\nabla\psi^*}(\nabla\psi(\cdot), \eta)].$$

Proof We will use the identity proved in Lem. 12.

$$\begin{aligned} g_{q_t, K}^* &= \mathbb{E}_{q_t} [\mathcal{M}_{p, \psi} K(\cdot, \theta)] \\ &= \mathbb{E}_{q_t} [K(\cdot, \theta) \nabla^2 \psi(\theta)^{-1} \nabla \log p(\theta) + \nabla_{\theta} \cdot (K(\cdot, \theta) \nabla^2 \psi(\theta)^{-1})] \\ &= \mathbb{E}_{q_t} [K(\cdot, \theta) \nabla^2 \psi(\theta)^{-1} \nabla_{\theta} (\log p_H(\nabla\psi(\theta)) + \log \det \nabla^2 \psi(\theta)) + \nabla_{\theta} \cdot (K(\cdot, \theta) \nabla^2 \psi(\theta)^{-1})] \\ & \hspace{15em} \text{(by change-of-variable formula)} \\ &= \mathbb{E}_{q_t} [K(\cdot, \theta) \nabla^2 \psi(\theta)^{-1} \nabla_{\theta} \log p_H(\nabla\psi(\theta)) + \sum_{i,j=1}^d [\nabla^2 \psi(\theta)^{-1}]_{ij} \nabla_{\theta_i} K(\cdot, \theta)_{:,j}] \\ & \hspace{15em} \text{(by applying Lem. 12 to each row of } K(\cdot, \theta)) \\ &= \mathbb{E}_{q_t} [K(\cdot, \theta) \nabla^2 \psi(\theta)^{-1} \nabla_{\theta} \log p_H(\nabla\psi(\theta)) + \sum_{j=1}^d \nabla_{\eta_j} K(\cdot, \theta)_{:,j}] \\ &= \mathbb{E}_{q_t, H} [K(\cdot, \nabla\psi^*(\eta)) \nabla \log p_H(\eta) + \sum_{j=1}^d \nabla_{\eta_j} K(\cdot, \nabla\psi^*(\eta))_{:,j}] \\ &= \mathbb{E}_{q_t, H} [K_{\nabla\psi^*}(\nabla\psi(\cdot), \eta) \nabla \log p_H(\eta) + \nabla_{\eta} \cdot K_{\nabla\psi^*}(\nabla\psi(\cdot), \eta)], \end{aligned}$$

where $A_{:,j}$ denotes the j -th column of a matrix A . \square

Lemma 12. For a strictly convex function $\psi \in C^2 : \mathbb{R}^d \rightarrow \mathbb{R}$ and any vector-valued $g \in C^1 : \mathbb{R}^d \rightarrow \mathbb{R}^d$, the following relation holds:

$$\nabla \cdot (\nabla^2 \psi(\theta)^{-1} g(\theta)) = \text{Tr}(\nabla^2 \psi(\theta)^{-1} \nabla g(\theta)) - g(\theta)^\top \nabla^2 \psi(\theta)^{-1} \nabla_\theta \log \det \nabla^2 \psi(\theta).$$

Proof By the product rule of differentiation:

$$\nabla \cdot (\nabla^2 \psi(\theta)^{-1} g(\theta)) = \text{Tr}(\nabla^2 \psi(\theta)^{-1} \nabla g(\theta)) + g(\theta)^\top \nabla \cdot (\nabla^2 \psi(\theta)^{-1}). \quad (21)$$

This already gives us the first term on the right side. Next, we have

$$\begin{aligned} & [\nabla^2 \psi(\theta)^{-1} \nabla \log \det \nabla^2 \psi(\theta)]_i \\ &= \sum_{j=1}^d [\nabla^2 \psi(\theta)^{-1}]_{ij} \text{Tr}(\nabla^2 \psi(\theta)^{-1} \nabla_{\theta_j} \nabla^2 \psi(\theta)) \\ &= \sum_{j=1}^d [\nabla^2 \psi(\theta)^{-1}]_{ij} \sum_{\ell, m=1}^d [\nabla^2 \psi(\theta)^{-1}]_{\ell m} [\nabla_{\theta_j} \nabla^2 \psi(\theta)]_{m\ell} \\ &= \sum_{j, \ell, m=1}^d [\nabla^2 \psi(\theta)^{-1}]_{ij} [\nabla^2 \psi(\theta)^{-1}]_{\ell m} \nabla_{\theta_j} \nabla^2 \psi(\theta)_{m\ell} \\ &= \sum_{j, \ell, m=1}^d [\nabla^2 \psi(\theta)^{-1}]_{ij} \nabla_{\theta_m} \nabla^2 \psi(\theta)_{j\ell} [\nabla^2 \psi(\theta)^{-1}]_{\ell m} \\ &= - \sum_{m=1}^d \nabla_{\theta_m} (\nabla^2 \psi(\theta)^{-1})_{im} \\ &= -[\nabla \cdot \nabla^2 \psi(\theta)^{-1}]_i. \end{aligned}$$

Plugging the above relation into (21) proves the claimed result. \square

Lemma 13 ([43, Lemma A.1]). Let A be a square matrix, and $0 < \epsilon < \frac{1}{2} \|A + A^\top\|_{\text{op}}$. Then,

$$\log |\det(I + \epsilon A)| \geq \epsilon \text{Tr}(A) - 2\epsilon^2 \|A\|_F^2,$$

where $\|\cdot\|_F$ denotes the Frobenius norm of a matrix.

Lemma 14. Let K be a matrix-valued kernel and \mathcal{H}_K be the corresponding RKHS. Then, for any $f \in \mathcal{H}_K$ (f is vector-valued), we have

$$\|f(x)\|_2 \leq \|f\|_{\mathcal{H}_K} \|K(x, x)\|_{\text{op}}^{1/2}, \quad \|\nabla f(x)\|_F^2 \leq \|f\|_{\mathcal{H}_K}^2 \sum_{i=1}^d \|\nabla_{x_i, x_i}^2 K(x, x')|_{x'=x}\|_{\text{op}},$$

where $\|\cdot\|_{\text{op}}$ denotes the operator norm of a matrix induced by the vector 2-norm.

Proof We first bound the $\|f(x)\|_2$ as

$$\begin{aligned} \|f(x)\|_2 &= \sup_{\|y\|_2=1} f(x)^\top y = \sup_{\|y\|_2=1} \langle f, K(\cdot, x)y \rangle_{\mathcal{H}_K} \leq \|f\|_{\mathcal{H}_K} \sup_{\|y\|_2=1} \|K(\cdot, x)y\|_{\mathcal{H}_K} \\ &= \|f\|_{\mathcal{H}_K} \sup_{\|y\|_2=1} (y^\top K(x, x)y)^{1/2} \leq \|f\|_{\mathcal{H}_K} \sup_{\|y\|_2=1} \sup_{\|u\|_2=1} (u^\top K(x, x)y)^{1/2} \\ &= \|f\|_{\mathcal{H}_K} \sup_{\|y\|_2=1} \|K(x, x)y\|_2^{1/2} = \|f\|_{\mathcal{H}_K} \|K(x, x)\|_{\text{op}}^{1/2}. \end{aligned}$$

The second result follows similarly,

$$\begin{aligned}
\|\nabla f(x)\|_F^2 &= \sum_{i=1}^d \|\nabla_{x_i} f(x)\|_2^2 = \sum_{i=1}^d \sup_{\|y\|_2=1} (\nabla_{x_i} f(x)^\top y)^2 = \sum_{i=1}^d \sup_{\|y\|_2=1} (\nabla_{x_i} \langle f, K(\cdot, x)y \rangle_{\mathcal{H}_K})^2 \\
&= \sum_{i=1}^d \sup_{\|y\|_2=1} (\langle f, \nabla_{x_i} K(\cdot, x)y \rangle_{\mathcal{H}_K})^2 \leq \|f\|_{\mathcal{H}_K}^2 \sum_{i=1}^d \sup_{\|y\|_2=1} \|\nabla_{x_i} K(\cdot, x)y\|_{\mathcal{H}_K}^2 \\
&= \|f\|_{\mathcal{H}_K}^2 \sum_{i=1}^d \sup_{\|y\|_2=1} (y^\top \nabla_{x_i, x_i}^2 K(x, x')|_{x=x'} y) \\
&\leq \|f\|_{\mathcal{H}_K}^2 \sum_{i=1}^d \sup_{\|y\|_2=1} \sup_{\|u\|_2=1} (u^\top \nabla_{x_i, x_i}^2 K(x, x')|_{x=x'} y) \\
&= \|f\|_{\mathcal{H}_K}^2 \sum_{i=1}^d \sup_{\|y\|_2=1} \|\nabla_{x_i, x_i}^2 K(x, x')|_{x=x'} y\|_2 \\
&= \|f\|_{\mathcal{H}_K}^2 \sum_{i=1}^d \|\nabla_{x_i, x_i}^2 K(x, x')|_{x'=x}\|_{\text{op}}.
\end{aligned}$$

□